

SPH simulation and experimental validation of the dynamic response of floating offshore wind turbines in waves

Zhe Tan ^{a,b}, Peng-Nan Sun ^{b,d,*}, Nian-Nian Liu ^{b,d}, Zhe Li ^c, Hong-Guan Lyu ^{b,d}, Rong-Hua Zhu ^a

^a Ocean College, Zhejiang University, Zhoushan, 316021, Zhejiang, China

^b School of Ocean Engineering and Technology, Sun Yat-sen University, Zhuhai, 519082, China

^c Nantes Université, École Centrale Nantes, CNRS, LHEEA, UMR 6598, F-44000, Nantes, France

^d Southern Marine Science and Engineering Guangdong Laboratory (Zhuhai), Zhuhai, 519080, China



ARTICLE INFO

Keywords:

Smoothed particle hydrodynamics
Floating offshore wind turbine
Mooring
Experimental validation

ABSTRACT

The SPH (smoothed particle hydrodynamics) method coupled with a mooring analysis program is adopted to investigate the accuracy of the SPH method in simulating the hydrodynamics of FOWTs (floating offshore wind turbines). Both experimental and numerical studies were conducted for a floating box and a scaled FOWT model interacting with multiple wave conditions. The SPH method is proven to be accurate in solving the motion of the floaters under multiple wave conditions, showing good consistency with the experimental data. In addition, the snapshots of the wave profile and the motions of the box and FOWT model are compared between SPH results and experiments. Finally, the application of the SPH method is extended to real-scale FOWT simulations. The motion response and mooring line force in the simulations are analyzed and show that the SPH method has the potential to be applied to real-scale FOWT hydrodynamics problems.

1. Introduction

To solve the energy and climate problems faced by human beings, countries all over the world are focusing on developing renewable energy, of which wind power is an important part. Onshore wind power technology has become mature, the market is saturated, and there are not many high-quality wind farms left. In this case, offshore wind power is becoming an important means of wind power generation by virtue of its high-quality wind resources and vast ocean area. Now quantities of nearshore fixed wind turbines are under construction or have been connected to the grid to generate electricity. While in the future, floating offshore wind turbines (FOWTs) in the deep sea utilizing better wind resources and larger ocean areas will become the focus of offshore wind power generation. However, in some circumstances, FOWTs could be subjected to extreme sea conditions, which leads to the threats of structural damage and even their overturning [1]. Therefore, it is necessary to evaluate their motion responses and environmental loads under multiple sea environments before launching, which can ensure the feasibility of the projects and reduce the cost. To this end, lots of experiments and numerical simulations were conducted. Considering the difficulty and cost of experiments, which makes successful experimental experience relatively scarce [2,3], numerical simulation is a

good way to investigate the hydrodynamic performance of various kinds of FOWTs, especially in the presence of extreme wave conditions, real-scale models, and the coupling effects of winds, currents, and waves [4].

At present, most of the methods used in the hydrodynamic simulations of FOWTs are mesh-based, including Morison's equation, potential flow theory, and computational fluid dynamics (CFD) tools. Softwares using these methods such as ANSYS AQWA, FAST, OpenFOAM, OrcaFlex, SIMA, and Bladed are widely used in the hydrodynamic simulation of FOWTs. Shi et al. [5] used ANSYS AQWA to study the hydrodynamic performance of the OO-Star semisubmersible FOWT platform under different wind and wave conditions. Han et al. [6] studied the dynamic responses of the WindStar TLP system under typical ocean environment conditions through the FAST code. Xue et al. [7] used the open-source platform OpenFOAM to calculate the wave response of the FOWT substructure considering the effect of a tuned liquid multicolumn damper. Yang et al. [8] used OrcaFlex to study the effect of the number of columns on the stability and hydrodynamic response of a semisubmersible FOWT. Chuang et al. [9] applied SIMA and FAST to investigate the mechanism in which the wave mean drift force and slow-drift wave excitation load influence the platform dynamics. There are also cases that use coupled methods to perform hydrodynamic analysis of FOWTs.

* Corresponding author. School of Ocean Engineering and Technology, Sun Yat-sen University, Zhuhai, 519082, China.

E-mail address: sunpn@mail.sysu.edu.cn (P.-N. Sun).

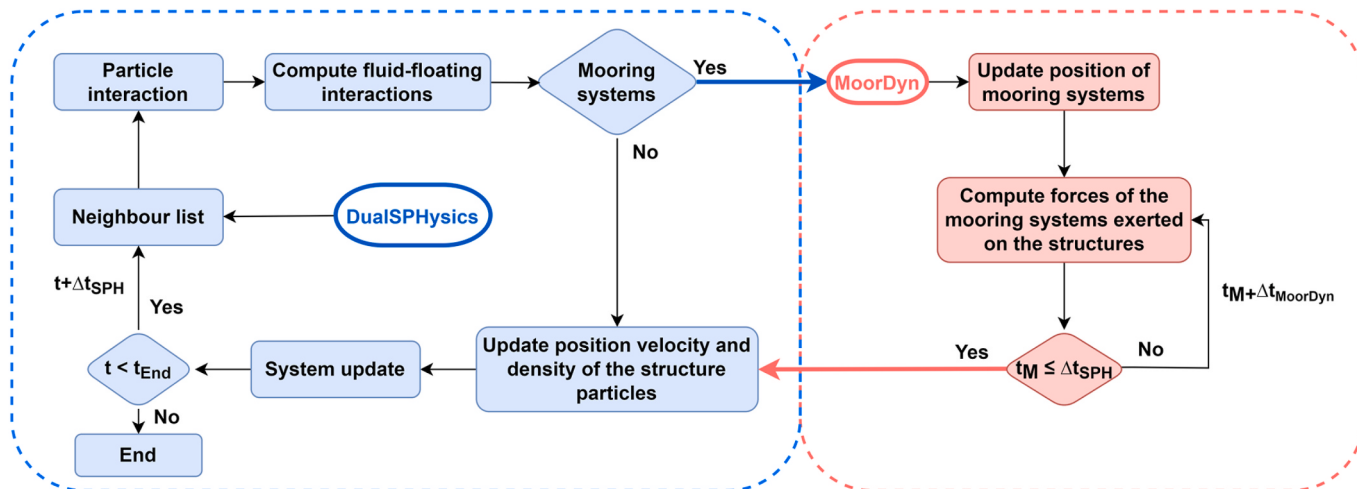


Fig. 1. Flow chart of the coupling process between DualSPHysics and MoorDyn (adapted from Ref. [56]).

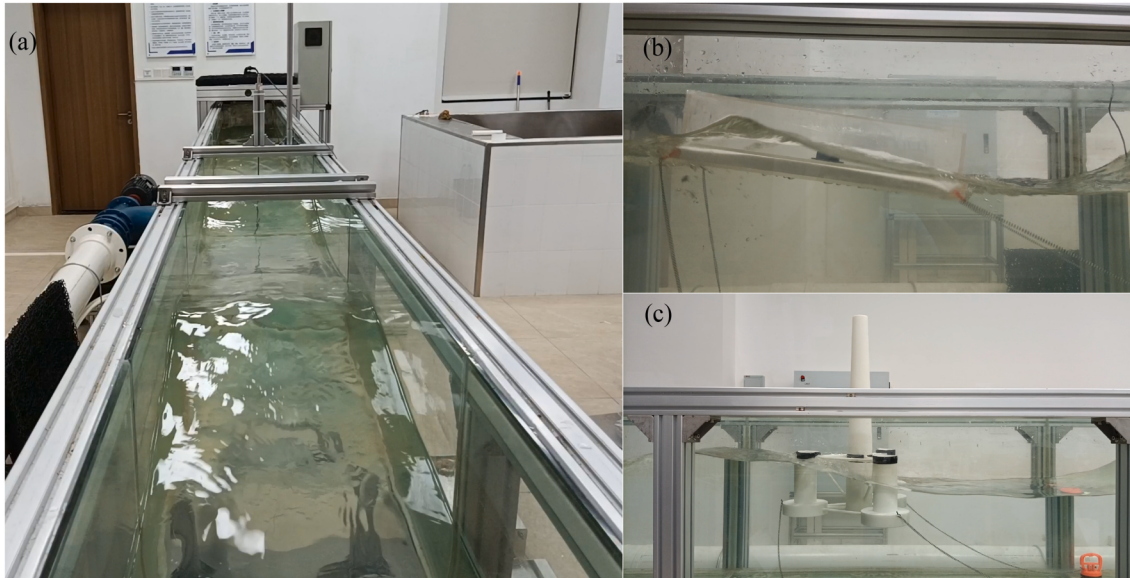


Fig. 2. Photographs of the flume (a), box (b), and FOWT model (c).

Table 1
Parameters of the motion sensor.

Parameter	Value
Measurement range of acceleration	±16 g
Measurement range of angular velocity	±2000°/s
Measurement range of angle range	±180° (X and Z); ±90° (Y)
Acceleration precision	0.01°/g
Angular velocity precision	0.05°/s
Sampling frequency	60 Hz

Yang et al. [10] used a coupled framework of FAST and AQWA (F2A) to analyze the transient dynamics of a 5 MW barge-type FOWT when one mooring line is suddenly broken under rated and extreme conditions. Some researchers have also combined OpenFOAM and MBDyn to use this fully coupled CFD-MBD tool to perform aerodynamic-fluid-mooring-elastic analysis of FOWTs [11]. Chen et al. [12] developed a coupled method for FOWT mooring systems analysis based on a finite-difference model of mooring lines, whose results were in good agreement with the open-source mooring analysis program MoorDyn. However, although mesh-based methods have been widely

Table 2
Parameters of the floating box.

Parameter	Value
Material	Acrylic sheet
Size	40 cm × 20 cm × 10 cm
Mass	4 kg
Center of mass (CM)	2.9 cm above the center of the underside
Draft	5 cm
Elasticity modulus	2.4 GPa
Roll inertia about CM	0.0183 kg · m ²
Pitch inertia about CM	0.0599 kg · m ²
Yaw inertia about CM	0.0712 kg · m ²

adopted in the hydrodynamic analysis of FOWTs, there are still some limitations in mesh-based methods when simulating the violent deformation and even breakup of the free surfaces and the movement and deformation of solid boundaries [13], which can appear in extreme sea conditions faced by FOWTs.

Compared with traditional mesh-based methods, the SPH (smoothed particle hydrodynamics) method is a truly mesh-free method, which

Table 3
Parameters of the mooring lines.

Parameter	Value
Material	304 stainless steel
Elasticity modulus	193 GPa
Density	7.93 g/cm ³ (20 °C)
Mass per unit length	0.0305 kg/m
Volume-equivalent diameter	0.002213 m
Length	0.6 m

discretizes the problem domain with particles that have no fixed connection, allowing the particles to move arbitrarily. The two main characteristics of the SPH method are the Lagrangian characteristic and the meshless particle characteristic, which determine that the SPH method has obvious advantages over traditional mesh-based methods in the research of severe convection, large deformation, and moving boundary problems [14,15]. Hence, using the SPH method to analyze the hydrodynamics of moored floating structures, including FOWTs, will be a novel and beneficial attempt based on its inherent advantages.

It has been rare to use the SPH method to analyze the hydrodynamics of FOWTs, and there have been few cases. Leble and Barakos [16] carried out a dynamic analysis of a FOWT based on the coupling of SPH and HMB2 CFD, which was used for the hydrodynamic simulation of the FOWT platform and the aerodynamic analysis of blades, respectively. Their results showed that the proposed weak coupling method can perform the analysis well. Besides, there have been some cases using the SPH method to perform hydrodynamic analyses of various kinds of moored floating structures. Ren et al. [17] used the SPH method to simulate the nonlinear interaction between waves and a moored floating breakwater, and the results showed that the dynamic response of the floating body of the simulation is in good agreement with existing experimental data. Similar work for a moored floating box can be referred to Ref. [18]. Some researchers conducted hydrodynamic simulations on different moored floating breakwaters using open-source

SPH solvers, DualSPHysics, or SPHysics, which are also consistent with the experiments [19–22]. Wei et al. [23] used the open-source SPH model, GPUSPH, and the open-source physics engine, Project Chrono, to solve the hydrodynamics of the wave energy device under wave-mooring conditions. Their results showed that the model can correctly predict the motion of the floating body and can be used to guide the design of the device. Crespo et al. [24] used DualSPHysics to simulate the interaction between waves and the wave energy device with an oscillating water column, and it showed that easy handling of moving objects inside the fluid is one of the main advantages of Lagrangian methods such as SPH. Wen et al. [25] proposed an improved SPH turbulent model to study the hydrodynamics of an oscillating water chamber, which can reproduce the free surface elevations both outside and inside the water chamber. Cleary and Rudman [26] used the SPH method to simulate the dynamic response of a semisubmersible platform with two different mooring systems under different wave conditions. Zhang et al. [27] used DualSPHysics to simulate the motion response of a moored mariculture platform under different sea states. All the cases above verify the applicability of the SPH method in the coupling analysis of offshore fluid-structure-mooring systems.

In these previous works, many SPH simulations of floating structures were two-dimensional, which needed fewer particles than three-dimensional SPH simulations, and then reduced the amount and time

Table 4
Wave parameters for the floating box.

Wave condition (WC)	Type	Period/s	Wave height/m
WC 1	Sine wave	1	0.1
WC 2	Sine wave	1	0.075
WC 3	Sine wave	1	0.05
WC 4	Sine wave	0.76	0.1
WC 5	Irregular wave (JONSWAP)	1.2 (Spectrum peak period)	0.1 (Significant wave height)

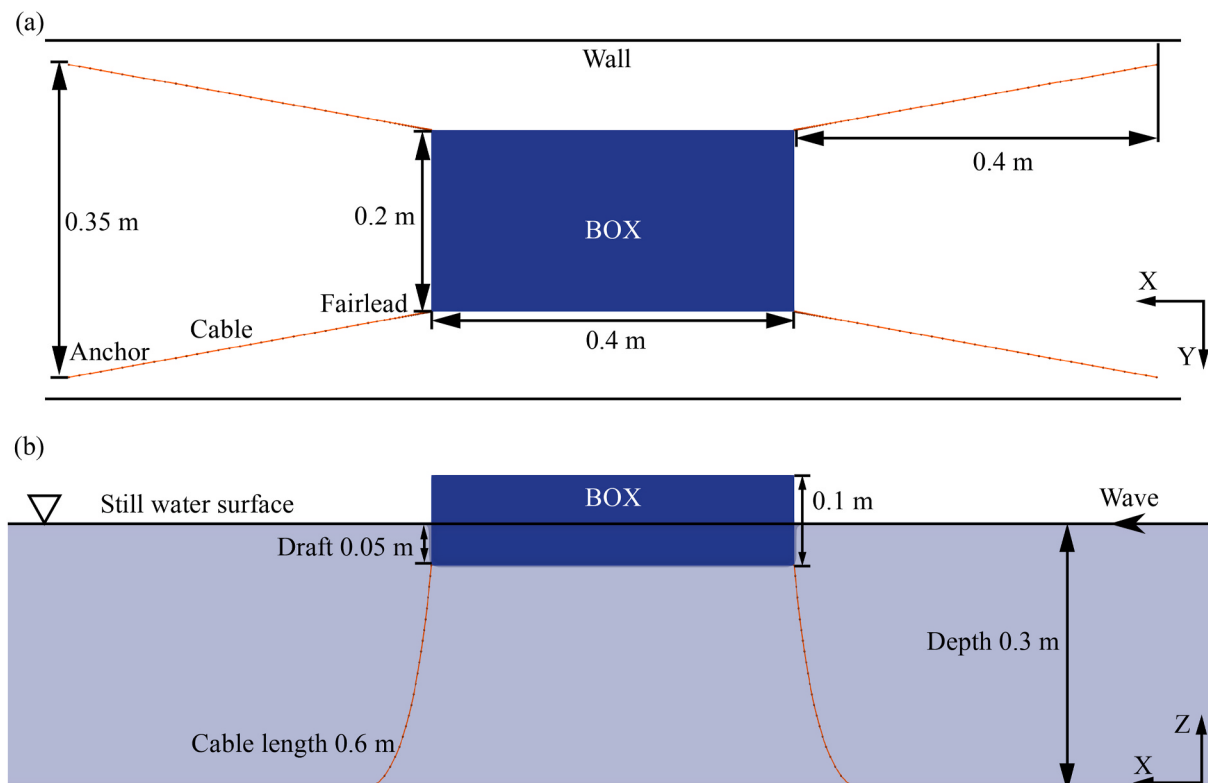


Fig. 3. The arrangements of the floating box and mooring lines. (a) Top view; (b) Front view.

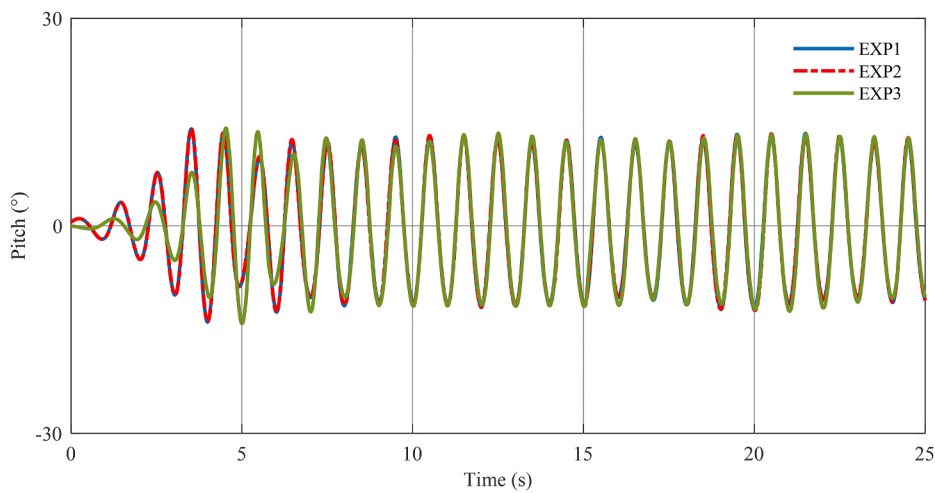


Fig. 4. Pitch angles of three repetitions of the experiment under WC 1.

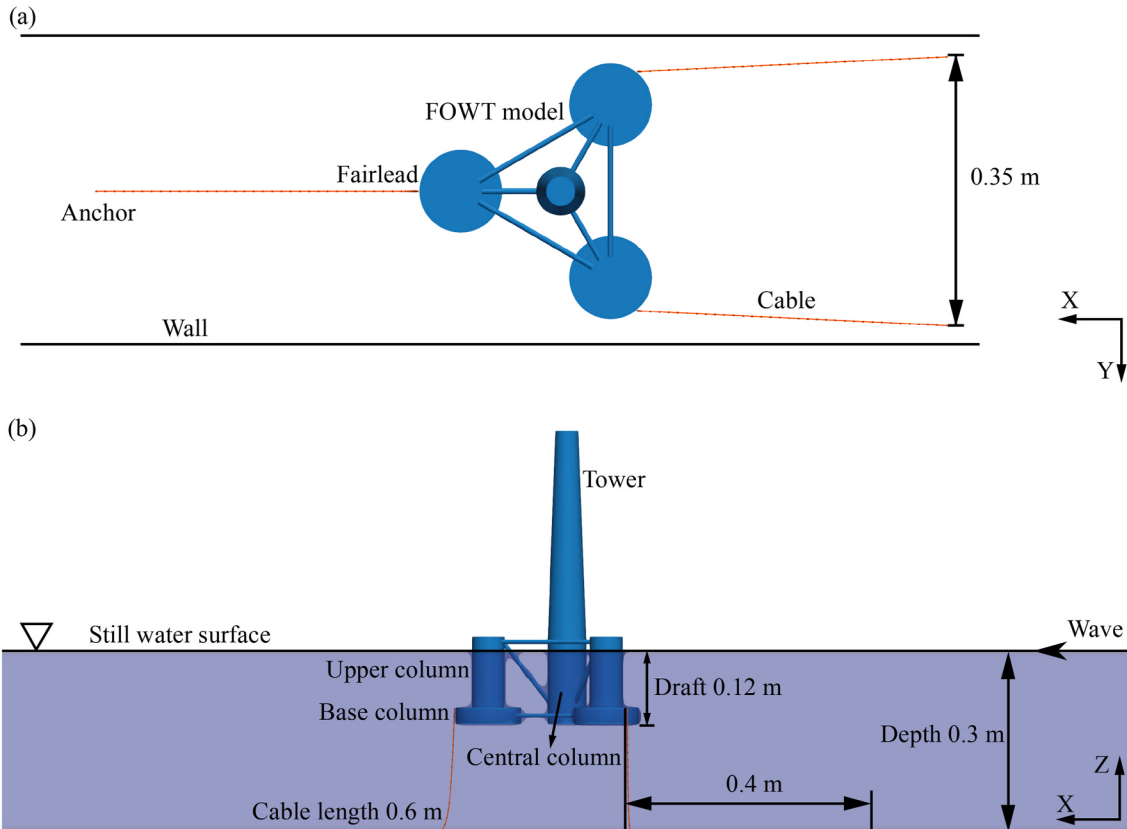


Fig. 5. The arrangements of the FOWT model and mooring lines. (a) Top view; (b) Front view.

Table 5
Wave parameters for the FOWT model.

Wave condition (WC)	Type	Period/s	Wave height/m
WC 1	Sine wave	1	0.1
WC 2	Sine wave	1	0.075
WC 3	Sine wave	1	0.05
WC 4	Sine wave	0.76	0.075
WC 5	Irregular wave (JONSWAP)	1.2 (Spectrum peak period)	0.05 (Significant wave height)

of computation. While in the present study, the six-degree-of-freedom motion of the moored floating bodies in three-dimensional space is simulated with the coupling between DualSPHysics and MoorDyn. In addition, thanks to the GPU-accelerating framework of DualSPHysics and an NVIDIA GEFORCE RTX 3090 GPU, millions of particles are generated to form a 3D numerical water tank to simulate the motion of the moored floating bodies under multiple wave conditions.

More importantly, the focus of the present research is to verify the accuracy of the SPH method in simulating the hydrodynamics of FOWTs in three-dimensional space. To this end, both experiments and simulations have been conducted and compared in the present work. With increasing complexity, experiments and simulations of a floating body

Table 6
Parameters of the FOWT model.

Parameter	Value
Length of tower	380 mm
Diameter of tower	41 mm (top), 69 mm (bottom)
Length of the central column	147 mm
Diameter of the central column	69 mm
Spacing between offset columns	245 mm
Length of upper (offset) columns	127 mm
Diameter of upper (offset) columns	59 mm
Length of base (offset) columns	29 mm
Diameter of base (offset) columns	117 mm
Diameter of pontoons and cross braces	8 mm
Overall height	527 mm
Draft	120 mm
Mass	2166 g
Center of mass	66 mm above the center of the central column bottom
Material	Resin
Elasticity modulus	2.6 GPa
Roll inertia about CM	0.0386 kg · m ²
Pitch inertia about CM	0.0386 kg · m ²
Yaw inertia about CM	0.0331 kg · m ²

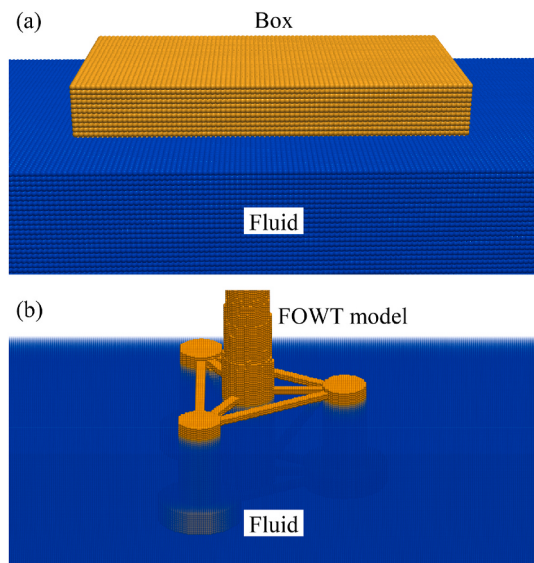


Fig. 6. Particle models of the floating bodies. (a) Box; (b) FOWT model.

Table 7
Interparticle distances and computation information (with an NVIDIA GEFORCE RTX 3090 GPU).

Interparticle distance/m	Total number of particles	Physical time/s	Computational time/h
0.005	2353336	5	1.58
0.003	10801420	5	11.2
0.0025	18539852	5	30.9

with a simpler structure, a box, were performed first to verify the applicability and accuracy of the coupled SPH simulation of the floating body, wave, and mooring system. Then, experimental and numerical studies on the hydrodynamics of a scaled FOWT model were conducted. These studies allow one to carry out two types of comparisons: one is the comparison between the experiments and simulations, and the other is the comparison between the simple structure, the box, and the complex structure, the FOWT model, which will show how the effectiveness changes for the SPH method when dealing with different structures.

After the above validation, real-scale simulations were conducted to explore the prospect of the SPH method applied in FOWT engineering analysis.

The rest of the paper is organized as follows: Section 2 introduces the numerical models used in this paper, including the SPH model and the way it couples with the mooring analysis. Section 3 presents the content of the experiments and SPH simulations. The validations of the SPH method for the experiments will be shown and analyzed here. Section 4 extends the SPH simulations of the scaled FOWT model to real-scale FOWT simulations. Finally, the main conclusions and future prospects are summarized in Section 5.

2. Numerical models

2.1. Brief recall of the SPH model

The SPH method was one of the earliest meshless methods proposed by Lucy, Gingold, and Monaghan in 1977 to solve large-scale astrodynamics problems [28,29], and was later used in solid and fluid mechanics. In the 1990s, the SPH method developed rapidly, and now it is widely applied in the field of hydrodynamics, involving multiphase flow [30,31], incompressible flow, fluid-structure interaction [32,33], free-surface flow [34,35], etc. In practical applications, it is used in ocean and coastal engineering [36], environmental conservation [37], biomechanics [38], and so on.

2.1.1. Governing equations

The SPH method discretizes the problem domain with particles that have no fixed connection. With the method of kernel approximation and particle approximation in SPH, the Lagrangian continuity equation with an density diffusive term and momentum equation can be discretized as [15,39]:

$$\begin{cases} \frac{d\rho_i}{dt} = \sum_j m_j \mathbf{v}_{ij} \cdot \nabla_i W(\mathbf{x}_i - \mathbf{x}_j, h) + 0.1 h c_0 \sum_j \psi_{ij} \cdot \nabla_i W(\mathbf{x}_i - \mathbf{x}_j, h) \frac{m_j}{\rho_j}, \\ \psi_{ij} = 2 \left(\rho_j^D - \rho_i^D \right) \frac{\mathbf{x}_i - \mathbf{x}_j}{\|\mathbf{x}_i - \mathbf{x}_j\|^2} \end{cases}, \quad (1)$$

$$\frac{d\mathbf{v}_i}{dt} = - \sum_j m_j \left[\left(\frac{p_i}{\rho_i^2} + \frac{p_j}{\rho_j^2} \right) + \Pi_{ij} \right] \nabla_i W(\mathbf{x}_i - \mathbf{x}_j, h) + \mathbf{g}, \quad (2)$$

where ρ_i and ρ_j denote the density of the fluid particle i and j respectively; m_j denotes the mass of the fluid particle j ; \mathbf{v}_{ij} is the velocity vector difference between particle i and particle j , i.e. $\mathbf{v}_{ij} = \mathbf{v}_i - \mathbf{v}_j$; W is the kernel function; \mathbf{x} denotes the position of the particles; h is the smoothing length of W and is chosen as $h = 1.25\Delta x$ in this study where Δx is the particle spacing; c_0 is the artificial speed of sound; the superscript D denotes the dynamic density or pressure; p_i and p_j are the pressure at particle i and particle j respectively; Π_{ij} is the artificial viscosity term; \mathbf{g} is the gravitational acceleration.

The smoothing function used in this study is [40]:

$$W(r, h) = \frac{21\pi h^3}{16} \left(1 - \frac{q}{2} \right)^4 (2q + 1), \quad 0 \leq q \leq 2, \quad (3)$$

where $q = r/h$, and r denotes the distance between a targeted particle and its neighbors within the support domain.

The artificial viscosity, Π_{ij} , is used to suppress the numerical non-physical oscillations caused by shock waves, and is written as [41]:

$$\begin{cases} \frac{-\alpha \bar{c}_{ij} \mu_{ij}}{\bar{\rho}_{ij}}, & \mathbf{v}_{ij} \cdot \mathbf{x}_{ij} < 0 \\ 0, & \mathbf{v}_{ij} \cdot \mathbf{x}_{ij} \geq 0 \end{cases}, \quad (4)$$

and $\mu_{ij} = \frac{h \mathbf{v}_{ij} \cdot \mathbf{x}_{ij}}{|\mathbf{x}_{ij}|^2 + \eta^2}$,

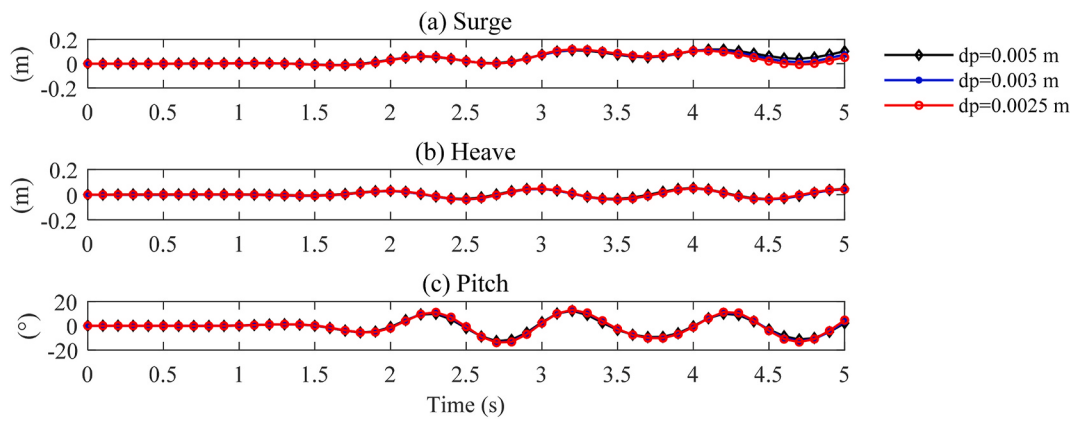


Fig. 7. The motion of the floating box under different interparticle distances. (a) Surge; (b) Heave; (c) Pitch.

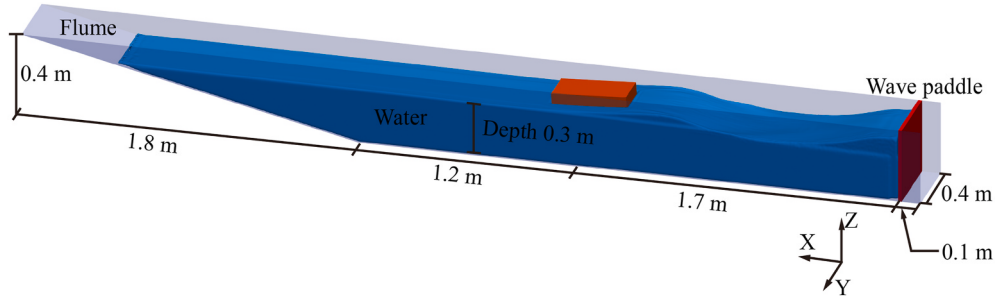


Fig. 8. Numerical flume used for the floating box under regular wave conditions.

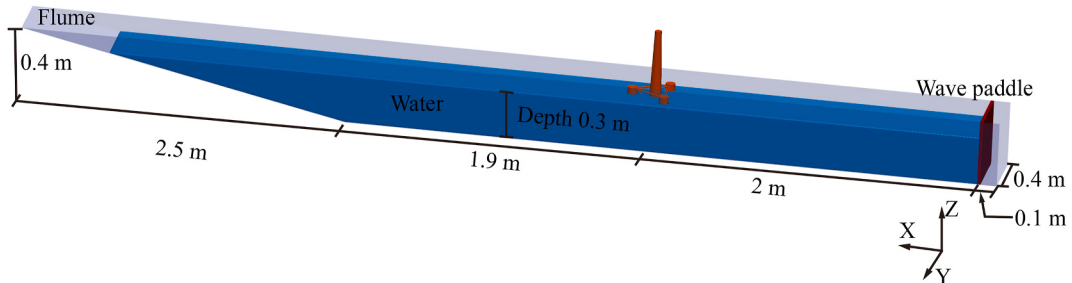


Fig. 9. Numerical flume used for the scaled FOWT model under regular wave conditions.

Table 8
SPH simulation parameters.

Parameter	Value
Gravitational acceleration	-9.81 m/s ²
Density of water	1000 kg/m ³
Physical time	25 s
Interparticle distance for the floating box	0.005 m
Interparticle distance for the FOWT model	0.003 m

where α is a coefficient; $\bar{c}_{ij} = (c_i + c_j)/2$ is the mean speed of sound; $x_{ij} = x_i - x_j$; $\eta^2 = 0.01h^2$.

Equation of state is used to describe the relationship between fluid pressure and density in the SPH method, which is expressed as [42]:

$$P = b \left[\left(\frac{\rho}{\rho_0} \right)^\gamma - 1 \right]; \quad b = c_0^2 \rho_0 / \gamma, \quad (5)$$

where $\rho_0 = 1000 \text{ kg/m}^3$ is the reference density for water; γ is the polytropic coefficient of fluid, which is usually chosen as 7 for water flow;

Table 9
Parameters of the mooring lines in the simulations.

Parameter	Value
Line stiffness	$7.42 \times 10^5 \text{ N}$
Bottom stiffness constant	$3 \times 10^6 \text{ Pa/m}$
Bottom damping constant	$3 \times 10^5 \text{ Pa/m}$
Transverse added mass coefficient	1
Tangential added mass coefficient	0
Transverse drag coefficient	1.6
Tangential drag coefficient	0.05
Number of discrete nodes of a mooring line	50

$c_0 = \sqrt{(\partial P / \partial \rho)}|_{\rho_0}$ is the artificial sound speed of the fluid, and it is set as 36.8 m/s and 43.8 m/s for the simulations of the floating box and FOWT model respectively.

2.1.2. Boundary conditions

The free-surface boundary condition can be directly satisfied in the weakly compressible SPH method [43], while the treatment of the wall

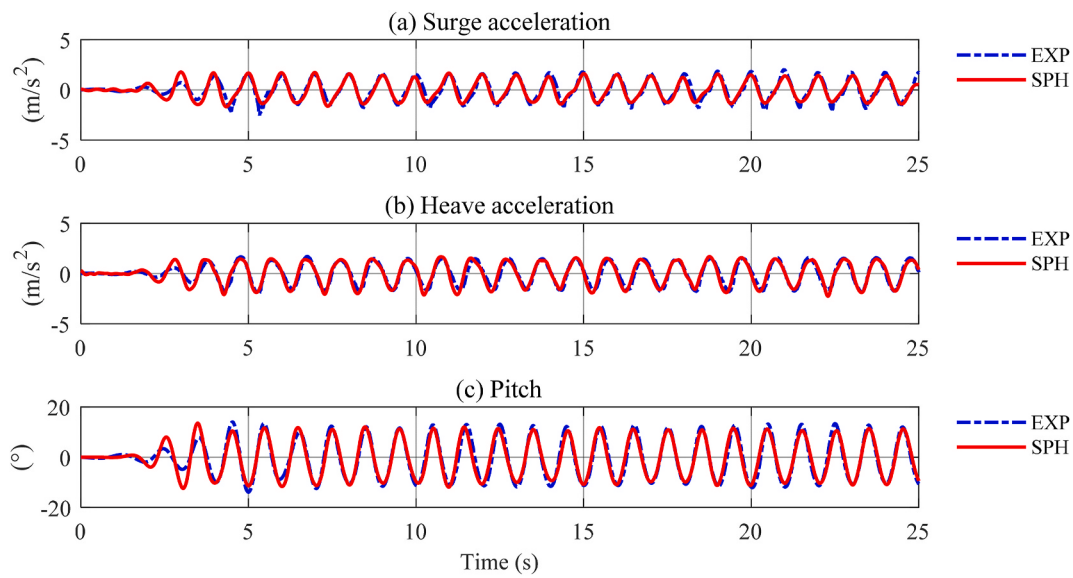


Fig. 10. Motion of the floating box under WC 1. (a) Surge acceleration; (b) Heave acceleration; (c) Pitch.

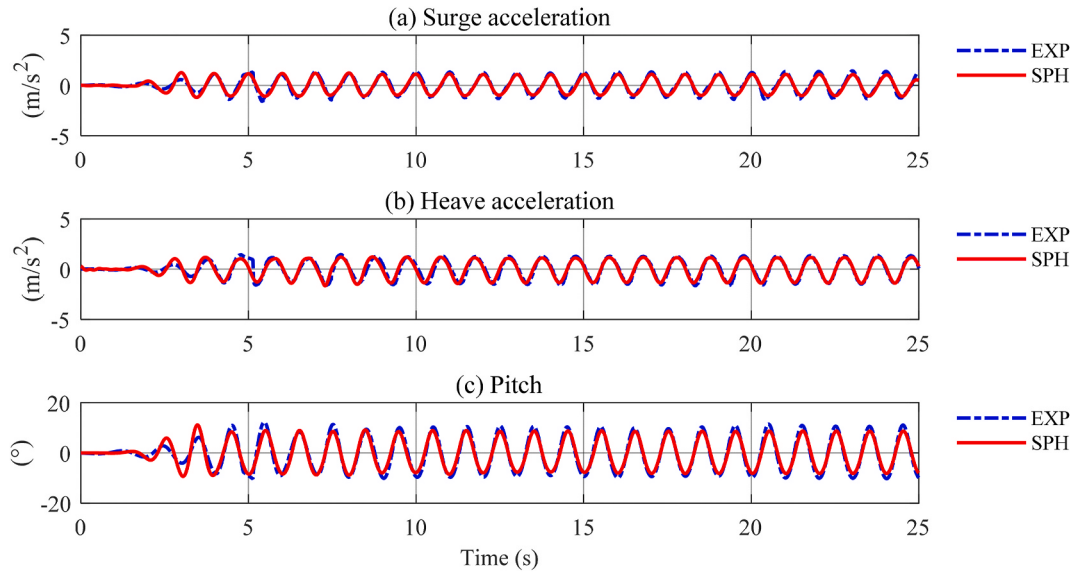


Fig. 11. Motion of the floating box under WC 2. (a) Surge acceleration; (b) Heave acceleration; (c) Pitch.

boundary condition directly affects the solution accuracy of the whole flow field. Due to the approximation in the meshless SPH method, the interpolation of one of the functions at a given point may not be exactly accurate, so the correct treatment of the wall boundary condition is very important for the solution accuracy. There are some methods to deal with the wall boundary condition, such as the mirror particle method, also called the ghost particle method [44,45], which generates ghost particles symmetrically about the wall boundary to fluid particles near the boundary. These ghost particles have the same physical properties as real particles, but their velocities are in opposite directions due to the mirroring, thus preventing the non-physical penetration of the boundary. Besides, Adami et al. [46] proposed a method to obtain the dynamic solid boundary condition with fixed ghost particles, directly from the flow field interpolation, simplifying the application of the method.

The Dynamic Boundary Condition (DBC) is the default method used in DualSPHysics and hence is adopted in this study [47]. The boundary particles are treated as fluid particles and satisfy the same equations in this method, but they do not move like the fluid particles. Instead, they

either remain at a fixed position or move as artificially specified.

2.1.3. Fluid-rigid body motion

The floating body is treated as a rigid body when computing its motion driven by waves and mooring lines. The governing equations for the motion of the floating body are written as [48]:

$$\begin{cases} M\dot{\mathbf{U}} = \mathbf{Mg} + \mathbf{F}, \mathbf{U} = \dot{\mathbf{X}}_R, \\ I_R\dot{\Omega}_R = \mathbf{T}_R, \Omega_R = \theta \end{cases}, \quad (6)$$

where \mathbf{U} and Ω_R are the velocity and angular velocity around the pivotal point, R , respectively; θ and X denotes the angle of rotation and position of the body; M and I_R are the total mass and moment of inertia about the point R . The force \mathbf{F} and torque \mathbf{T} consist of both the hydrodynamic and the mooring line forces. More details regarding treating the interaction between the floating body and fluid can be found in Refs. [48,49].

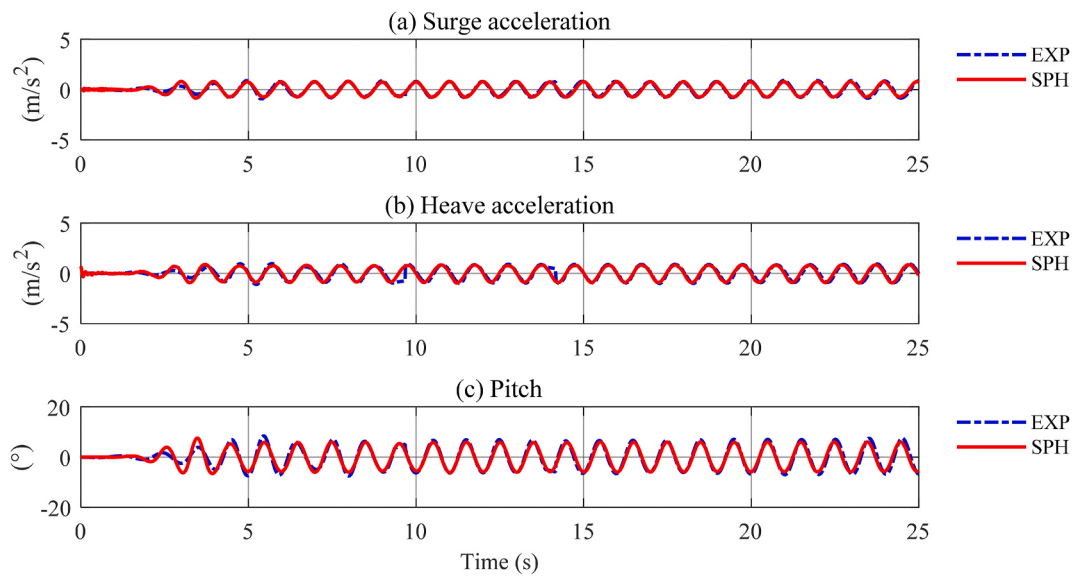


Fig. 12. Motion of the floating box under WC 3. (a) Surge acceleration; (b) Heave acceleration; (c) Pitch.

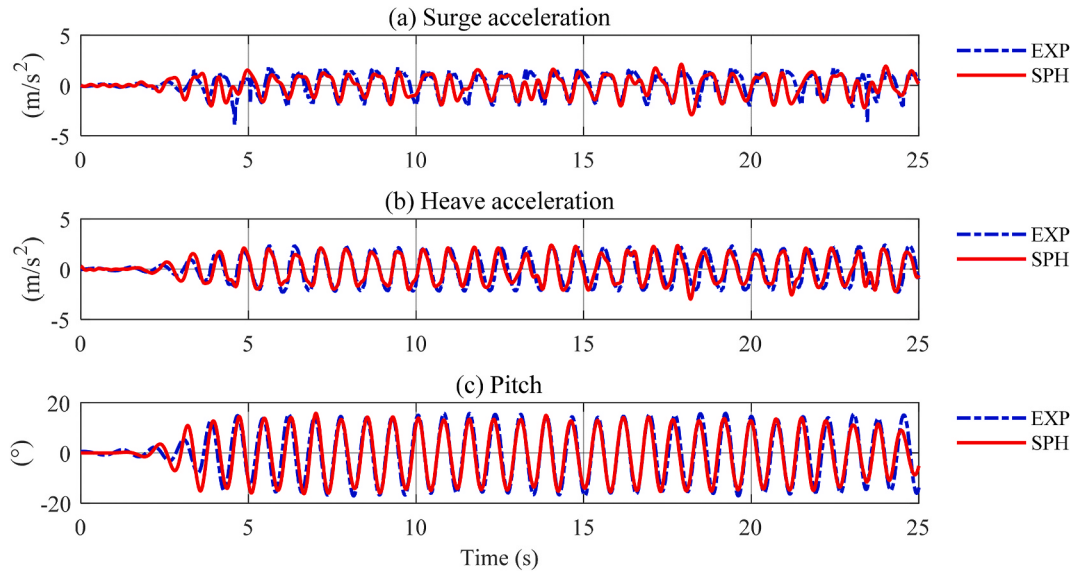


Fig. 13. Motion of the floating box under WC 4. (a) Surge acceleration; (b) Heave acceleration; (c) Pitch.

2.1.4. Time integration and parallel computation

In the SPH method, the time integration of the discretized SPH equations can be performed using methods such as the Runge-Kutta, leap-frog, predictor-corrector schemes, etc [50]. No matter which time integration scheme is adopted, the Courant-Friedrichs-Lowy (CFL) condition should be respected to make the explicit time integration stable. In the SPH scenario, the time step, Δt , is usually determined according to the minimum smooth length in the SPH simulation, i.e.

$$\Delta t = CFL \min\left(\frac{h_i}{c}\right) \quad (7)$$

It should be noted that directly adopting Eq. (7) in SPH simulations should be avoided because it could somewhat lead to instability when local flow velocities are over-large. To prevent this issue, the calculation of the time step should consider the evolutions of the flow field. In this paper, following the suggestions by Monaghan and Kos [42], the time step is determined by taking the viscosity dissipation and external forces into account, which yields:

$$\Delta t_{cv} = \min\left(\frac{h_i}{c_i + 0.6(\alpha_{\prod} c_i + \beta_{\prod} \max(\mu_{ij}))}\right), \quad (8)$$

$$\Delta t_f = \min\left(\frac{h_i}{f_i}\right)^{\frac{1}{2}}, \quad (9)$$

where α_{\prod} and β_{\prod} are two constants depending on specific problems; f_i is the magnitude of the force acting on per unit mass. Finally, the time step used in SPH simulations is given as:

$$\Delta t = CFL \min(\Delta t_{cv}, \Delta t_f), \quad (10)$$

where CFL is adopted as 0.4 in this paper.

The GPU implementation in the DualSPHysics code is mainly focused on force computation [51]. The parallel GPU computing techniques greatly speed up the solving process, especially when the number of particles is huge, and make the simulations under multiple conditions

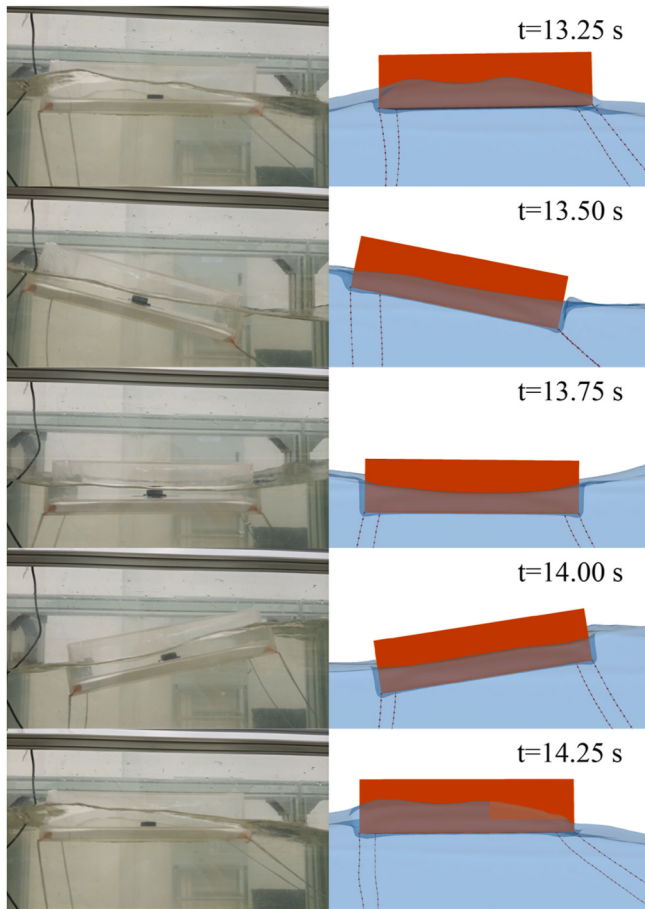


Fig. 14. Snapshots of the floating box in the experiment (left) and simulation (right) under WC 1 in a complete period.

with millions of particles in this study possible. More details about the GPU implementation in DualSPHysics can be found in Refs. [52,53].

2.2. Coupling between the SPH method and mooring analysis

The lumped-mass method is a common method used in mooring line

modeling, which discretizes mooring lines into point masses connected by linear spring-damper segments [54]. In the open-source mooring analysis program, MoorDyn, which is based on the lumped-mass method, the cable model combines internal axial stiffness, damping forces with weight, buoyancy forces, hydrodynamic forces from Morrison's equation, and forces from contact with the seabed, and these forces compose the equation of motion for each node of the mooring line [55].

MoorDyn can be coupled to the open-source SPH solver, DualSPHysics, enabling the mooring analysis in the SPH method. During the coupling process shown in Fig. 1, the motion data initially solved in DualSPHysics is transferred to MoorDyn and used as input for the mooring computation; MoorDyn then solves the mooring line dynamics, updates the positions of the mooring line segments, and calculates the forces at the fairlead connections; these data are then transferred to DualSPHysics, and these additional external forces are then added into the final resulting force acting on the floating structure, which is used to calculate the final motion of it [54].

3. Experimental and numerical studies

3.1. Experimental campaigns

In this part, experiments on the interaction between moored floating structures and waves are conducted in a wave flume at Sun Yat-sen University for validating the SPH simulations. Photographs of the flume, box, and FOWT model are shown in Fig. 2. The flume used in the experiments is 16 m long, 0.4 m wide, and 0.5 m high, and the water depth is 0.3 m. And there is a piston for wave generation and a wave absorber in the flume. The floating structures include a floating box and a scaled FOWT model. The experiments focus on the six-degree-of-freedom motion of the floating structures, and the experimental data are obtained by a motion sensor for analysis. The parameters of the motion sensor are shown in Table 1. The results of the experiments will be shown together with that of the SPH simulations for comparison.

3.1.1. Experiments of the floating box

The parameters of the floating box are shown in Table 2. Four mooring lines were used to moor the floating box in the experiments, whose parameters are shown in Table 3. The distance between the center of gravity of the box and the wave paddle is 5 m, and the detailed arrangements of the floating box and mooring lines are illustrated in

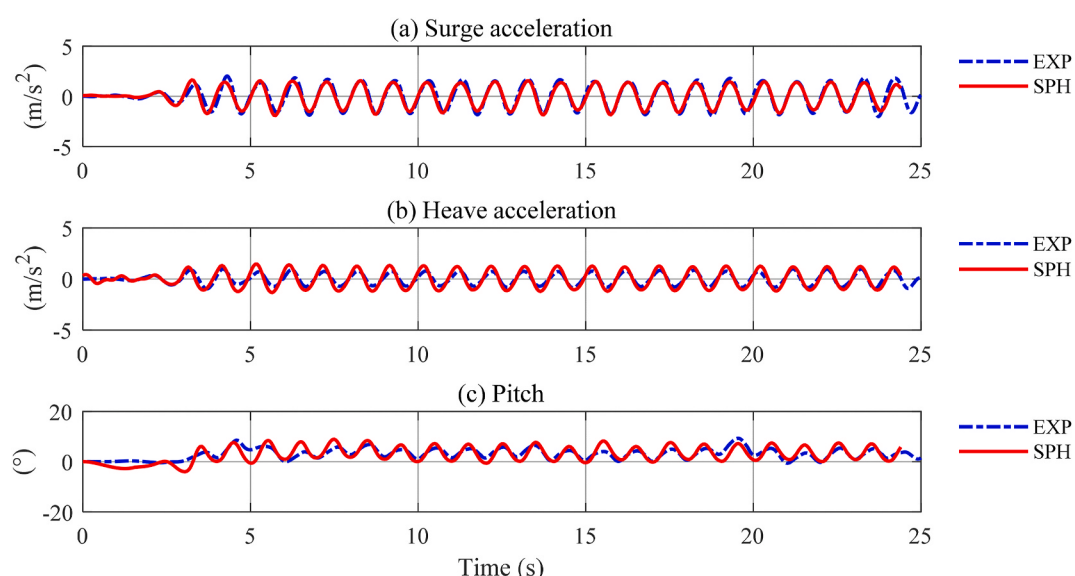


Fig. 15. Motion of the scaled FOWT model under WC 1. (a) Surge acceleration; (b) Heave acceleration; (c) Pitch.

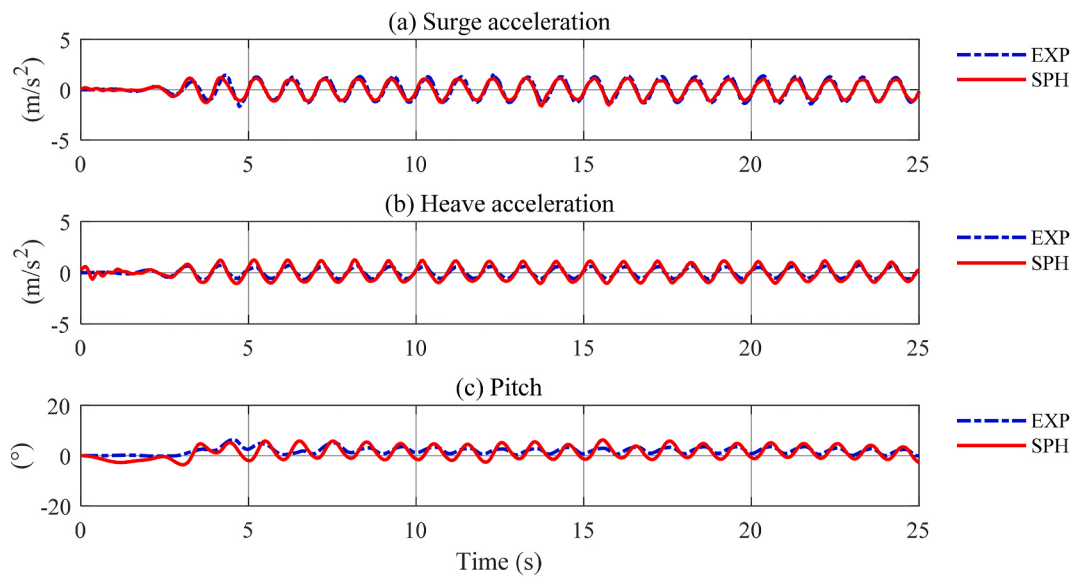


Fig. 16. Motion of the scaled FOWT model under WC 2. (a) Surge acceleration; (b) Heave acceleration; (c) Pitch.

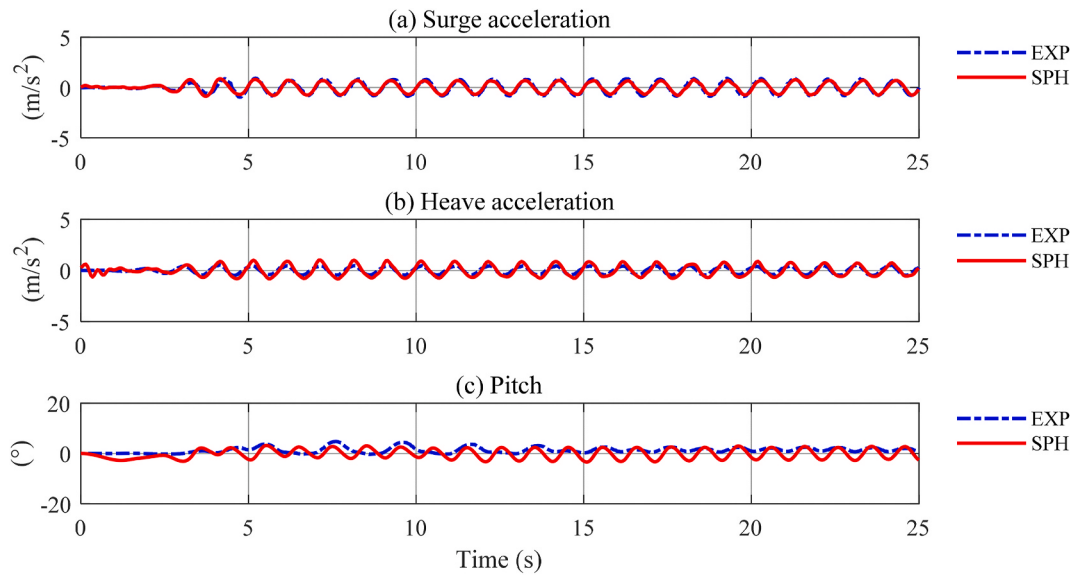


Fig. 17. Motion of the scaled FOWT model under WC 3. (a) Surge acceleration; (b) Heave acceleration; (c) Pitch.

Fig. 3. Multiple wave conditions were set to interact with the floating box. And the parameters of the waves are presented in [Table 4](#).

A motion sensor was used to collect the motion data of the floating box in six degrees of freedom, including accelerations and angles in the X, Y, and Z directions in the experiments. The angles in X, Y, and Z directions are used to describe the roll, pitch, and yaw of the floating box respectively. While for surge, heave, and sway, the accelerations in X, Y, and Z directions are used instead of the displacements because integrating the accelerations discretely twice to obtain the displacements amplifies the error, which results in a deviation from the actual displacement of the floating box. Since DualSPHysics can directly output the accelerations along each axis during the simulations, the acceleration data in the experiments will be a better choice to make comparisons. In addition, data of surge, heave, and pitch is analyzed with emphasis while data of sway, roll, and yaw is not analyzed in this study for the motion of the three degrees of freedom is not salient.

The motion data collected in the experiments is based on the local coordinate system of the sensor itself. To analyze the motion of the

floating box, the motion data of the local coordinate system should be converted to the global coordinate system which is fixed to the flume. Due to the layout of the experimental apparatus, the generation and propagation of waves are all symmetrical about the central longitudinal section of the flume, the movement of the floating box also approximates symmetrical about the section, and its yaw, sway, and roll motion amplitude is small. Therefore, ignoring the motion in the three degrees of freedom when converting the data can simplify the conversion algorithm. The conversion algorithm for the surge, pitch, and heave motion data is as follows:

$$\begin{cases} a_x = a_{xl} \cos(\text{ang}_{yl}) + a_{zl} \sin(\text{ang}_{yl}) \\ a_z = a_{zl} \cos(\text{ang}_{yl}) - a_{xl} \sin(\text{ang}_{yl}) \end{cases}, \quad (11)$$

where a_x and a_z are the acceleration of the floating box along the x and z axes in the global coordinate system, i.e., the surge acceleration and the heave acceleration respectively; a_{xl} and a_{zl} are the acceleration of the floating box along the x and z axes in the local coordinate system of the sensor respectively; ang_{yl} is the pitch angle of the floating box, which

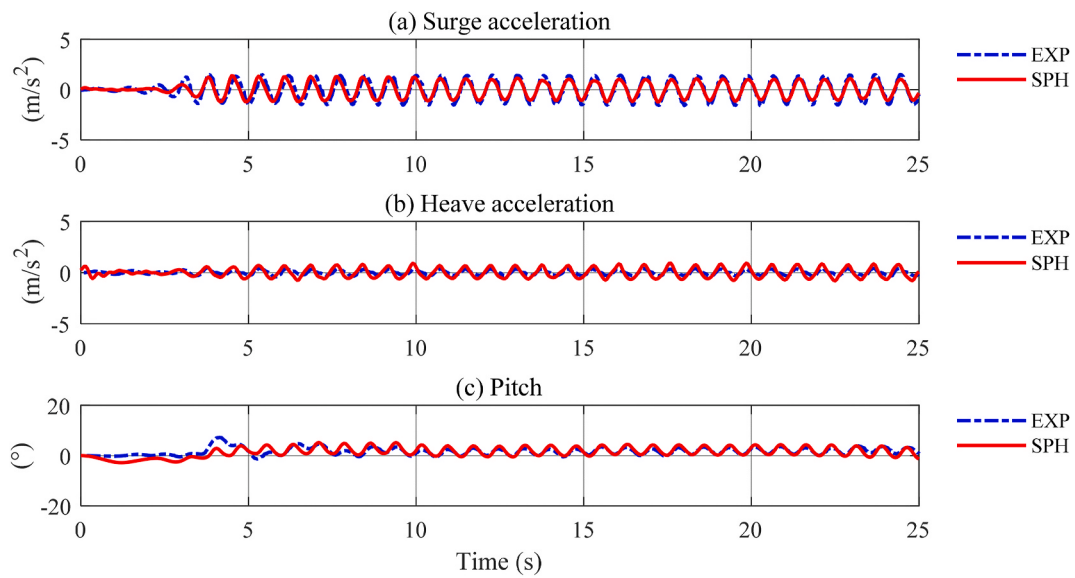


Fig. 18. Motion of the scaled FOWT model under WC 4. (a) Surge acceleration; (b) Heave acceleration; (c) Pitch.

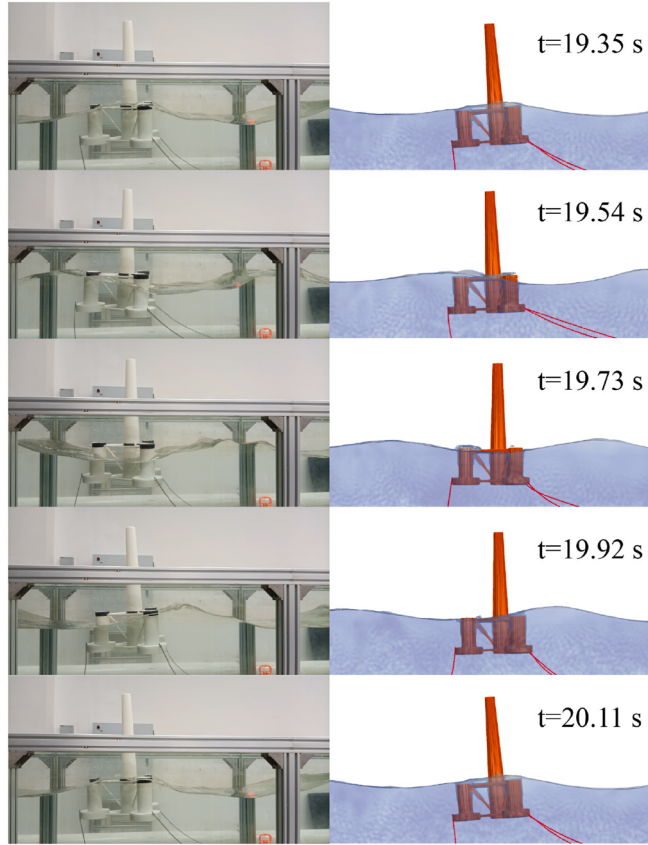


Fig. 19. Snapshots of the FOWT model in the experiment (left) and simulation (right) under WC 4 in a complete period.

does not need to be converted between the two coordinate systems.

The experiment under WC 1 was repeated three times to analyze whether the experiments were reliable and the pitch angles of the box were chosen to be compared among the five repetitions. The result in Fig. 4 shows that the pitch angles of the three repetitive experiments are consistent with each other, especially in the second half of the time when the motion of the box becomes stable. It proves that the mode of the

experiments, from the implementation of the experiments to data collection and processing, is reliable and that the data is stable for analysis.

3.1.2. Experiments of the scaled FOWT model

The experiments of the scaled FOWT model represent the interaction between complex structures and fluid. The model was built based on the NREL OC4-DeepCwind system [57], which is a semisubmersible FOWT with a central column and three offset columns. Since only the interaction between the FOWT model and water is studied in the experiments, the turbine blades are omitted in the modeling, and the size of the model and its components is adjusted to the size of the flume. The model consists of a tower and a floating platform which is composed of a central column and three sets of offset columns. Each offset column includes an upper column and a base column. The detailed parameters of the model are shown in Table 6. The distance between the center of gravity of the FOWT model and the wave paddle is 5 m, and the detailed arrangements of the FOWT model and mooring lines are shown in Fig. 5. Properties of the mooring lines can be referred to in Table 3. The fairleads are spaced 120° apart. The direction of the mooring lines is approximately parallel to the direction of the pool wall due to the size limitation of the flume. Several wave conditions were set to interact with the FOWT model and the parameters of the waves are presented in Table 5.

3.2. SPH simulations, validations, and discussions

The open-source SPH solver, DualSPHysics, coupled with the open-source mooring analysis program, MoorDyn, is used to simulate the interaction between two moored floating bodies with waves in three-dimensional space. The simulations are compared with the experiments to validate the accuracy of the SPH method. Most settings in the simulations, such as the arrangements and mass properties of the floating bodies, wave conditions, and mooring system properties, are the same as the experiments above, but the flume length is shortened under the regular wave conditions to save the number of particles and improve computational efficiency. The same geometries of the floating bodies as the experiments are used in the simulations, which are composed of particles (see Fig. 6) and involved in the simulations.

3.2.1. Convergence analysis

Interparticle distance defines the distance between particles. For the

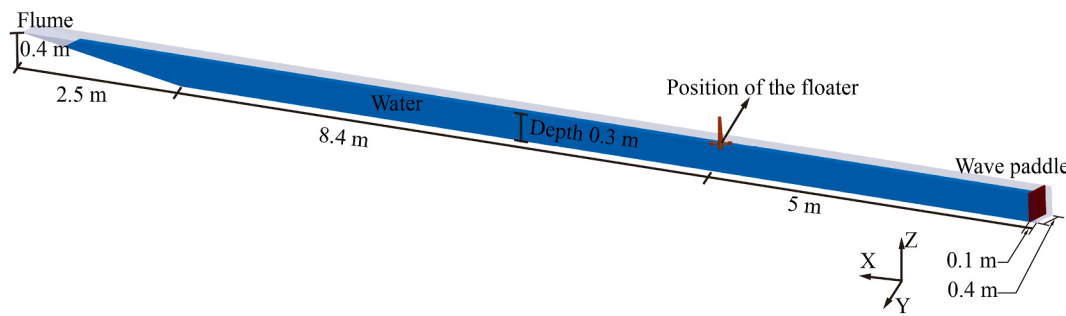


Fig. 20. Numerical flume used for the floater under irregular wave conditions.

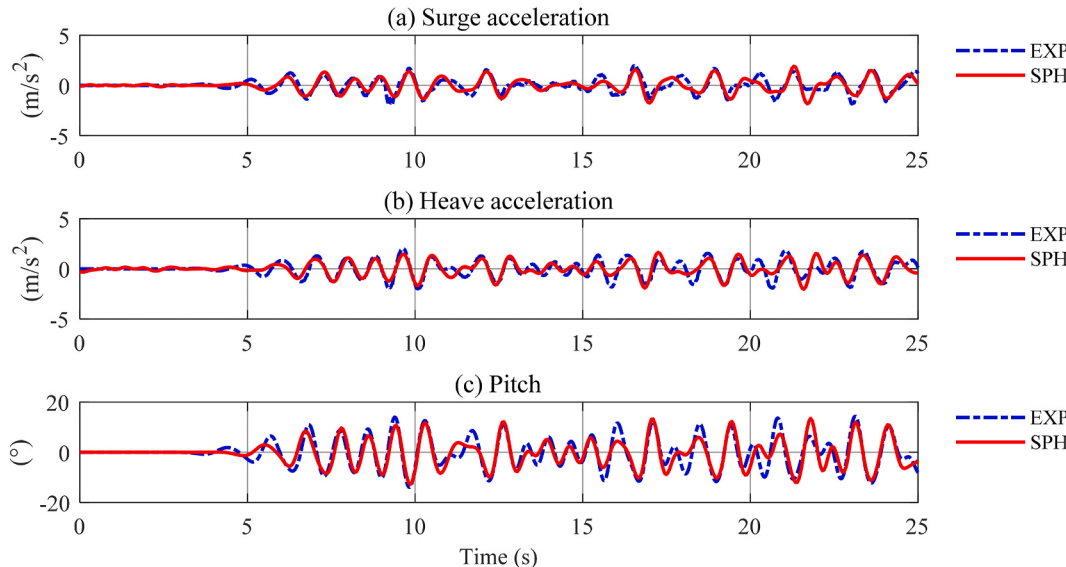


Fig. 21. Motion of the floating box under WC 5. (a) Surge acceleration; (b) Heave acceleration; (c) Pitch.

same flow field size, the smaller the interparticle distance is, the more particles are generated and the finer the flow field is discretized. Generally speaking, a smaller interparticle distance can make the simulation more accurate, but it will lead to the rapid growth of computation amount and time. In this section, three interparticle distances are set, and the simulation results under different interparticle distances will be compared to determine the appropriate interparticle distances for subsequent simulations by considering both the accuracy and computation time. Simulations for convergence analysis simulate the motion of the floating box under WC 1. The interparticle distances and the corresponding computation information are shown in Table 7. It shows that the total number of particles and the computation time increase rapidly as the interparticle distance decreases. The motion of the floating box obtained from the simulations with different interparticle distances is shown in Fig. 7. It can be seen that there's not much difference among the motion data under different interparticle distances. According to the results above, interparticle distance, 0.005 m, will be used for subsequent simulations of the floating box under regular wave conditions, which can ensure an appropriate compromise between the accuracy and the computational time. And the interparticle distance is set as 0.003 m for the FOWT model under regular wave conditions because it has more complex structures than the box and needs better discretization precision.

3.2.2. Simulations and validations under regular wave conditions

The numerical flumes used in the SPH simulations of the floating box and FOWT model under regular wave conditions are illustrated in Fig. 8 and 9. The simulation parameters are shown in Table 8. The parameters

of the mooring lines needed in the simulations are shown in Table 9. The SPH simulation results include the surge acceleration, heave acceleration, and pitch angle of the floaters under each regular wave condition. Simulations and experimental motion data of the floating box will be compared in Fig. 10 (WC 1), Fig. 11 (WC 2), Fig. 12 (WC 3) and Fig. 13 (WC 4). And simulations and experimental motion data of the FOWT model will be compared in Fig. 15 (WC 1), Fig. 16 (WC 2), Fig. 17 (WC 3) and Fig. 18 (WC 4). Due to the high-frequency numerical noise generated in some cases during the computation of the SPH method, especially for acceleration signals that are sensitive to high frequencies, we use low-pass filtering on acceleration data from the simulations to make it better to be presented and the cut-off frequency is 4 Hz.

In Fig. 10 (WC 1), Fig. 11 (WC 2), Fig. 12 (WC 3) and Fig. 13 (WC 4), the surge and heave acceleration under one wave condition have the same order of magnitude, and all the pitch angles are within the range of -20° – 20° . Under the periodic wave conditions, the surge and heave acceleration and pitch angle show obvious periodicity. The floating box has different motions under different wave conditions. Under WC 1, WC 2 and WC 3, the wave heights are 0.1 m, 0.075 m, and 0.05 m respectively. Moreover, as the wave height decreases, amplitudes of the surge and heave acceleration, and pitch angle all decrease, but still maintain the same periodicity of 1 s. Compare Fig. 10 (WC 1) with Fig. 13 (WC 4), the motion of the floating box has different periodicity under different wave periods, and the accelerations and pitch angle are larger when the wave period is 0.76 s than when the wave period is 1 s.

Under the regular wave conditions, the surge and heave accelerations and pitch angles of the SPH simulations are very close to the experimental data, and the figure lines of the SPH simulations and

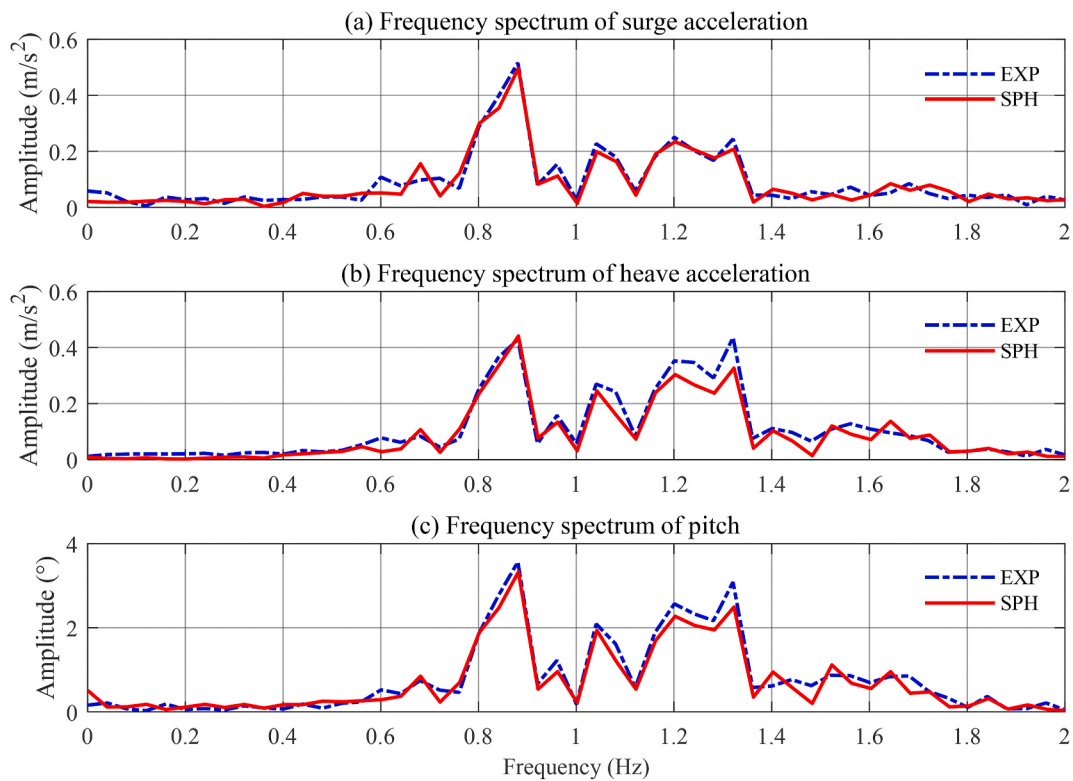


Fig. 22. Frequency spectrum of the (a) surge and (b) heave acceleration and (c) pitch of the floating box under WC 5.

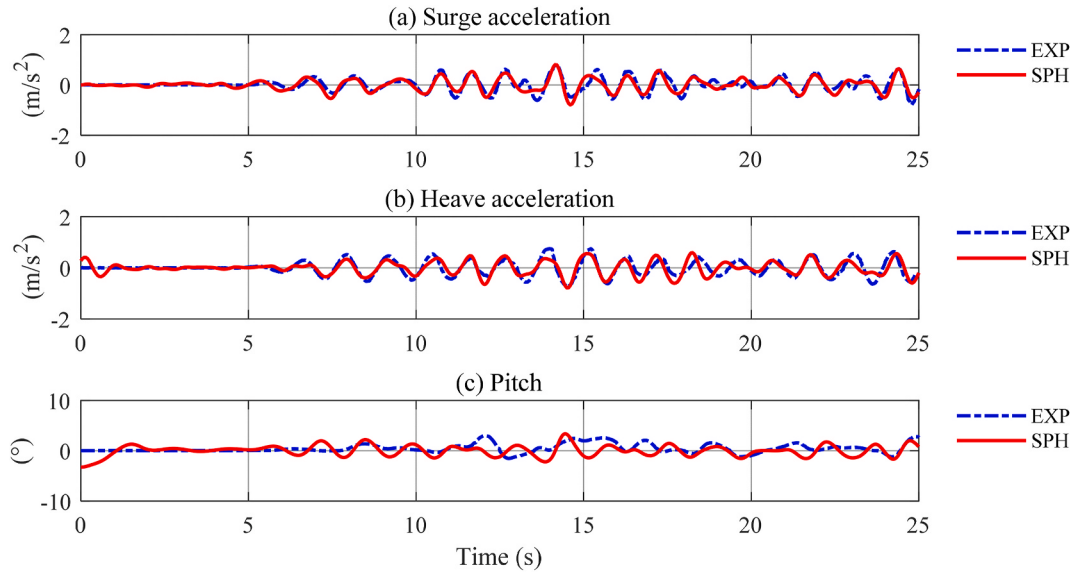


Fig. 23. Motion of the scaled FOWT model under WC 5 (a) Surge acceleration; (b) Heave acceleration; (c) Pitch.

experiments almost overlap. These results prove that DualSPHysics based on the SPH method has good accuracy in solving the motion of the moored floating box under regular wave conditions.

Apart from the data, snapshots of the floating box in the experiment and simulation under WC 1 in a complete period from 13.25 s to 14.25 s are compared in Fig. 14. The left and right column of the figure shows the experimental and simulation pictures respectively. From the top to the bottom of the figure is the process of the floating box from the wave crest to the wave trough and back to the wave crest again. The SPH simulation not only gives the accurate motion response and attitude of the floating box but also simulates the deformation of the free surface

well.

The motion of the scaled FOWT model has similar characteristics to that of the floating box, which is not going to be further discussed here. In Fig. 15 (WC 1), Fig. 16 (WC 2), Fig. 17 (WC 3) and Fig. 18 (WC 4), we can observe that the surge and heave accelerations of the scaled FOWT model in the SPH simulations under the regular wave conditions are in good agreement with the experimental results, with consistent amplitude and phase, and the figure lines are close to overlapping. Under the regular wave conditions, WC 1, WC 2, and WC4, the pitch angles of the scaled FOWT model in the simulations are consistent with that in the experiments. The amplitudes of the pitch angles of the simulations and

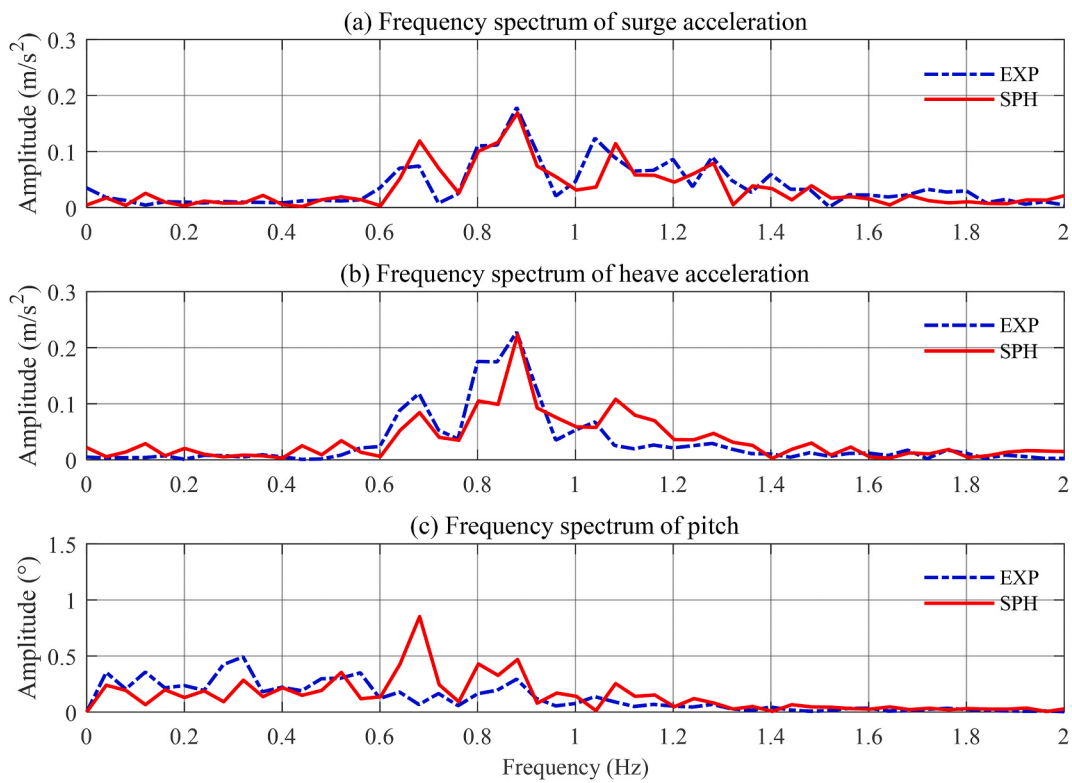


Fig. 24. Frequency spectrum of the (a) surge and (b) heave acceleration and (c) pitch of the FOWT model under WC 5.

Table 10
Mass properties of the FOWT.

Parameter	Value
Mass	$1.7372 \times 10^7 \text{ kg}$
Roll inertia about CM	$8.803 \times 10^9 \text{ kg} \cdot \text{m}^2$
Pitch inertia about CM	$8.803 \times 10^9 \text{ kg} \cdot \text{m}^2$
Yaw inertia about CM	$1.5808 \times 10^{10} \text{ kg} \cdot \text{m}^2$

Table 11
Wave parameters for the real-scale FOWT simulations.

Wave condition (WC)	Type	Period/s	Wave height/m
WC 1	Second-order Stokes wave	10	5
WC 2	Second-order Stokes wave	10	10
WC 3	Second-order Stokes wave	10	15

The motion of the real-scale FOWT in surge, heave, and pitch are shown in Fig. 27.

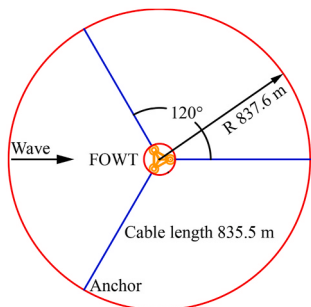


Fig. 25. Real-scale FOWT and mooring system.

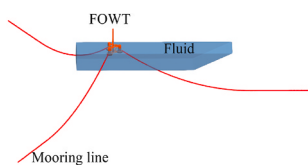


Fig. 26. Flow field and the mooring system.

experiments are basically the same in the second half of the time when the motion of the FOWT model becomes stable. Under WC 3, the local maxima of the pitch angle are close to the experimental value in the second half of the time, while the local minima are smaller than the experimental value. This is because the discrete precision of the particles gradually becomes insufficient as the wave height decreases from WC 1 to WC 3.

Snapshots of the FOWT model in the experiment and simulation under WC 4 in a complete period from 19.35 s to 20.11 s are compared in Fig. 19. The left and right column of the figure shows the experimental and simulation pictures respectively. From the top to the bottom of the figure is the process of the scaled FOWT model from the wave crest to the wave trough and back to the wave crest again. It can be seen that the picture obtained from the simulation is in agreement with the experimental snapshot. In the experiment, the wave crosses over the offset columns of the platform, and Fig. 19 shows that the simulation simulates this phenomenon well, which is the inherent advantage of SPH as a Lagrangian method to deal with large deformation of the free surface.

3.2.3. Simulations and validations under irregular wave conditions

Since the SPH method requires a large amount of computation, we shorten the length of the numerical flume to reduce the number of particles generated under regular wave conditions, thus reducing the amount of computation. And the SPH simulations have good consistency with corresponding experiments. While under irregular wave

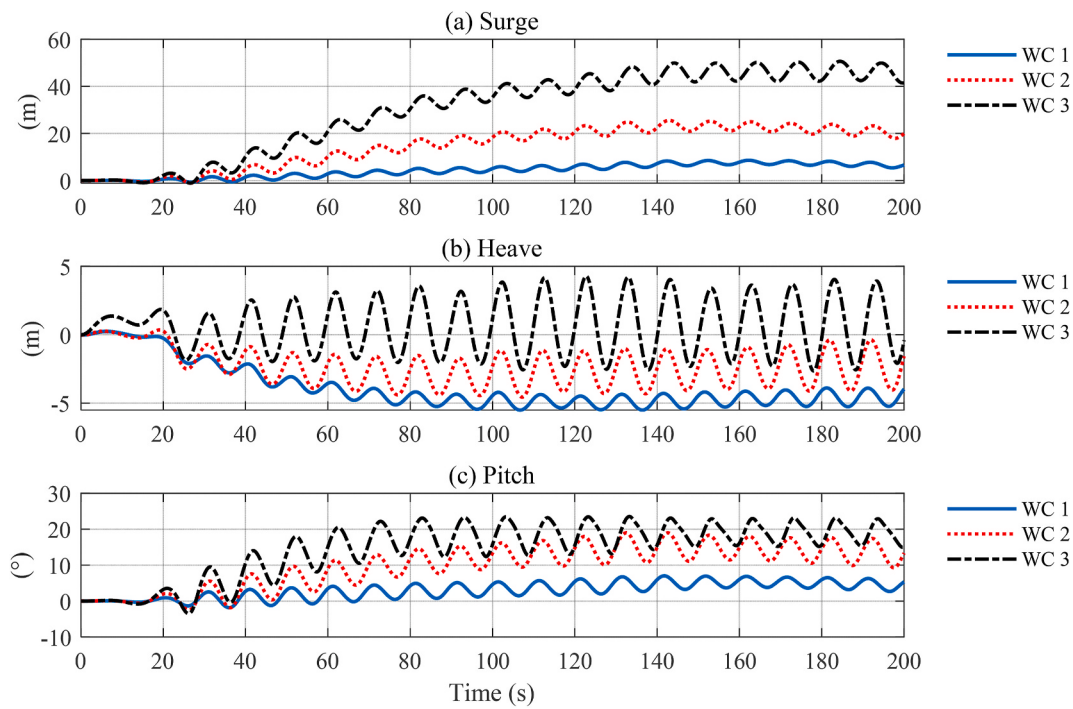


Fig. 27. Motion of the real-scale FOWT under three wave conditions. (a) Surge; (b) Heave; (C) Pitch.

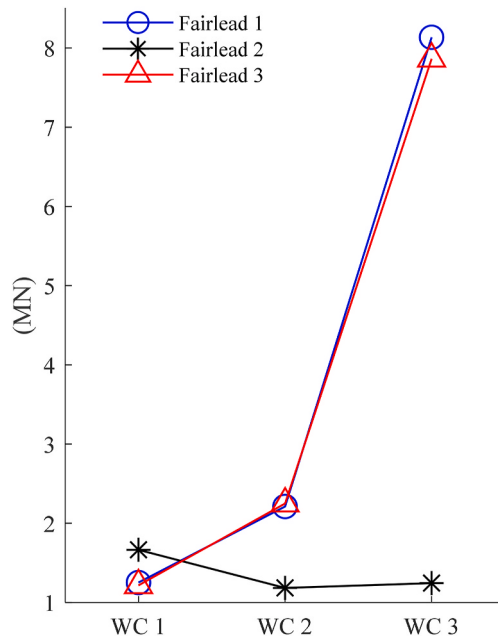


Fig. 28. Maximum force on Fairleads.

conditions, shortening the length of the numerical flume has an impact on the reflection and diffraction of irregular waves in the flume, thus affecting the motion of the floating body. Therefore, we use the same length for the numerical and experimental flumes under the irregular wave conditions, which is 16 m. And the floaters' distance away from the wave paddle is both set to 5 m, which is also the same as the experiments. The interparticle distance is 0.004 m, to keep the number of generated particles within the computational power of our GPU as the numerical flume becomes longer. The other parameters are the same as previous simulations under regular wave conditions. The numerical flume used for the floating box and FOWT model under irregular wave

conditions is illustrated in Fig. 20.

As shown in Fig. 21, the motion of the box in the simulation under the irregular wave condition has good consistency with the experiment. The motion of the box in the frequency domain is shown in Fig. 22, where the box movement is mainly concentrated in the frequency range of 0.6 Hz–1.4 Hz, and the frequency spectrum of the simulation is consistent with the experiment.

For the FOWT model, as shown in Fig. 23, the SPH results of surge and heave accelerations as well as the pitch angles under the irregular wave condition also agree fairly with the experiment. In the frequency spectrum of the FOWT model in Fig. 24, the frequencies of the motions are mainly concentrated in the range of 0.6 Hz–1.4 Hz. Especially for the surge and heave accelerations, the maximum amplitudes at the frequency of 0.88 Hz are the same between the experiment and SPH simulation.

Generally, the motions of the floaters in different wave conditions can be properly simulated by the present SPH model. Concerning the slight deviation of the pitch motion of the FOWT model between the experiment and simulation under the irregular wave condition, the numerical error is mainly due to the more complex shape of the FOWT model. The present particle spacing used to discretize the FOWT model is not small enough to represent the small structure details. In future studies, on one hand, the technique of multi-particle resolution should be adopted to locally refine the particles near the FOWT model; on the other hand, the multi-GPU parallel computation will be utilized to support the SPH simulation with more particles.

4. Extension to real-scale FOWT simulations

In this chapter, based on the SPH simulation of wave interaction with moored floating structures in the flume, the application of the SPH method is extended to real-scale FOWT simulations. Extreme wave conditions are set to explore the prospects of the application of the SPH method to the analysis of real-scale ocean engineering problems in high sea states.

The NREL 5 MW OC4-DeepCwind system is used in the real-scale simulations. As the simulations only consider the interaction between the platform and waves, blades and nacelle are ignored in modeling. The

size and mooring system properties of the OC4-DeepCwind system can be referred to Ref. [57]. Mass properties are adjusted and presented in Table 10. An illustration of the FOWT and mooring system is in Fig. 25.

For the SPH real-scale simulation, the size of the flow field and the interparticle distance have a large impact. The size of the mooring system occupies a major part of the system in this case, and if the flow field size is set at a 1-km level according to the distribution of the mooring lines, the flow field is bound to be too large. And even if too many particles are generated, the flow field cannot be discretized with good precision. Since the mooring lines are simulated using the lumped-mass method and do not directly interact with the fluid particles, the flow field size will be reduced to around the FOWT without changing the mooring system properties to reduce the number of particles while improving the discrete precision of the flow field. The length, width, and depth of the flow field are set to 740 m, 120 m, and 80 m with an interparticle distance of 1 m, and a mooring system with the same mooring parameters as described in Fig. 25 is generated. In Fig. 26, the fluid does not surround the mooring lines, but it does not affect the data transfer between the SPH solver and the mooring solver. Wave conditions used in the real-scale SPH simulations are presented in Table 11. The simulation duration is 200 s.

As can be seen from Fig. 27, under the interaction with periodic waves, the motion of the FOWT gradually tends to be stably periodic. From WC 1 to WC 3, the time required for surge and pitch to be stably periodic becomes longer, and the time required for heave to be stably periodic becomes shorter. With the wave height increasing from 5 m (WC 1) to 15 m (WC 3), the motion response in the surge, heave, and pitch quickly increases with obvious nonlinearity. In WC 3, the maximum surge of the FOWT is 50.7 m, the maximum heave is 64.3 m, and the maximum pitch is 23.5°. The motion response is too huge for the FOWT to work normally.

Fig. 28 shows the variation of the maximum force on each fairlead with the wave conditions. For every 5-m increase in wave height, the force on waveward fairleads increases rapidly with evident nonlinearity. The maximum force of the fairleads in WC 3 is 8.13 MN, which is about 4 times the value in WC 2, which indicates that the increase of wave height in high sea states will pose great challenges to the mooring system.

In short, the SPH method can provide reasonable results for the simulation of real-scale FOWT hydrodynamics, and can simulate the change of the motion response and mooring line force when the sea state becomes worse. It has the potential to be applied to real-scale ocean engineering problems.

5. Conclusions and prospects

In this study, the SPH method coupled with a mooring analysis program is adopted to investigate the accuracy of the SPH method in simulating the hydrodynamics of FOWTs. Both experiments and simulations were conducted for a floating box and a scaled FOWT model. The motion data of the experiments and simulations under the same wave conditions are obtained to be compared, which shows good consistency. Besides, the application of the SPH method is further extended to real-scale FOWT simulations. A flow field with mooring lines exposed outside is used to reduce the size of the flow field and the number of particles. Motion response and mooring system load of the real-scale FOWT are analyzed. The main conclusions of this paper are summarized as follows.

- (1) The SPH method shows good accuracy in solving the motion of the moored floating box and FOWT model under multiple regular wave conditions. It not only gives the accurate motion response of the floaters but also simulates the deformation of the free surface well. Besides, proper shortening of the SPH numerical flume length for regular wave conditions can keep a good balance between accuracy and calculation amount.

- (2) Under the irregular wave conditions, the SPH method simulates the motion of the rectangular box accurately, and the motion of the FOWT model is also properly calculated even the structure of the latter is more complex.
- (3) In the flow field with mooring lines exposed outside, SPH simulations for a real-scale FOWT can be performed with fewer particles and time. The motion response and mooring line force in the simulations show that the SPH method has the potential to be applied to real-scale FOWT hydrodynamics problems.

Future works can be conducted with the following considerations to further enhance the capability of SPH simulations for FOWT hydrodynamics.

- (1) Taking the wind, current, and wave load into consideration is necessary. To that end, the technique of multi-field coupling can be feasible. The coupling of wind can be possibly achieved through two ways. One is adding air particles above the water particles and using a purely particle-based way to solve the problem, and the other is coupling the SPH method with other wind turbine aerodynamic algorithms or solvers, such as the actuator line model, OpenFAST, etc.
- (2) Smaller interparticle distances for the FOWT model simulations can be applied to further improve the simulation accuracy. To that end, the technique of multi-particle resolution can be adopted.
- (3) Applying multi-GPU parallel computing in the SPH solving process. With more computing power and less computation time, generating more particles to improve the solution accuracy can be possible.
- (4) For the simulations of real-scale FOWT in the open sea, the present SPH model can be coupled with a potential solver which is straightforward to implement the far field boundary condition.

CRediT authorship contribution statement

Zhe Tan: Formal analysis, Methodology, Software, Resources, Validation, Investigation, Visualization, Writing – original draft. **Peng-Nan Sun:** Conceptualization, Methodology, Software, Resources, Data curation, Funding acquisition, Writing – review & editing. **Nian-Nian Liu:** Writing – review & editing. **Zhe Li:** Methodology, Writing – review & editing. **Hong-Guan Lyu:** Writing – review & editing. **Rong-Hua Zhu:** Project administration, Writing – review & editing.

Declaration of competing interest

The authors declare that they have no known competing financial interests or personal relationships that could have appeared to influence the work reported in this paper.

Acknowledgment

This research is supported by: the Guangzhou Basic and Applied Basic Research Project (Grant No. 202102020371), the Science Foundation of Donghai Laboratory (Grant No. DH-2022KF0311), the National Natural Science Foundation of China (Grant No. 52171329); the Natural Science Foundation of Guangdong Province of China (Grant No. 2022A1515012084) and the Fundamental Research Funds for the Central Universities, Sun Yat-sen University (Grant No. 22qntd0601). The SPH simulations were carried out with the open-source code, Dual-SPHysics, to which the authors are most grateful. The code can be found at <http://www.dual.sphysics.org/>.

Appendix A. Supplementary data

Supplementary data to this article can be found online at <https://doi.org/10.1016/j.renene.2023.03.030>.

[org/10.1016/j.renene.2023.01.081](https://doi.org/10.1016/j.renene.2023.01.081).

References

- [1] M. Luo, M. Rubinato, X. Wang, X. Zhao, Experimental investigation of freak wave actions on a floating platform and effects of the air gap, *Ocean Eng.* 253 (2022) 111192.
- [2] Y. Dong, Y. Chen, H. Liu, S. Zhou, Y. Ni, C. Cai, T. Zhou, Q.a. Li, Review of study on the coupled dynamic performance of floating offshore wind turbines, *Energies* 15 (11) (2022).
- [3] F. He, J. Leng, X.Z. Zhao, An experimental investigation into the wave power extraction of a floating box-type breakwater with dual pneumatic chambers, *Appl. Ocean Res.* 67 (2017) 21–30.
- [4] B. Tagliafierro, M. Karimirad, I. Martínez-Estévez, J.M. Domínguez, G. Viccione, A.J.C. Crespo, Numerical assessment of a tension-leg platform wind turbine in intermediate water using the smoothed particle hydrodynamics method, *Energies* 15 (11) (2022).
- [5] W. Shi, R. Xue, X. Hou, H. Xiu, L. Zhang, Dynamic response on 10 MW semisubmersible floating offshore wind turbine, *Ship Eng.* 43 (10) (2021) 1.
- [6] Z.L. Han, Y.S. Zhao, J. Su, Y.P. He, Y.W. Xu, F. Wu, Z.Y. Jiang, On the hydrodynamic responses of a multi-column TLP floating offshore wind turbine model, *Ocean Eng.* 253 (2022).
- [7] M.-A. Xue, P. Dou, J. Zheng, P. Lin, X. Yuan, Pitch motion reduction of semisubmersible floating offshore wind turbine substructure using a tuned liquid multicolumn damper, *Mar. Struct.* 84 (2022).
- [8] H.S. Yang, A. Alkhabbaz, D.S. Edirisinha, W. Tongphong, Y.H. Lee, FOWT stability study according to number of columns considering amount of materials used, *Energies* 15 (5) (2022).
- [9] Z.J. Chuang, S.W. Liu, Y. Lu, Influence of second order wave excitation loads on coupled response of an offshore floating wind turbine, *Int. J. Nav. Archit. Ocean Eng.* 12 (2020) 367–375.
- [10] Y. Yang, M. Bashir, C. Li, J. Wang, Investigation on mooring breakage effects of a 5 MW barge-type floating offshore wind turbine using F2a, *Ocean Eng.* 233 (2021).
- [11] Y. Liu, Q. Xiao, Development of a fully coupled aero-hydro-mooring-elastic tool for floating offshore wind turbines, *J. Hydraul.* 31 (1) (2019) 21–33.
- [12] L. Chen, B. Basu, S.R.K. Nielsen, A coupled finite difference mooring dynamics model for floating offshore wind turbine analysis, *Ocean Eng.* 162 (2018) 304–315.
- [13] M.B. Liu, S.M. Li, On the modeling of viscous incompressible flows with smoothed particle hydrodynamics, *J. Hydraul.* 28 (5) (2016) 731–745.
- [14] A. Khayyer, H. Gotoh, Y. Shimizu, On systematic development of FSI solvers in the context of particle methods, *J. Hydraul.* 34 (3) (2022) 395–407.
- [15] M.B. Liu, G.R. Liu, Smoothed particle hydrodynamics (SPH): an overview and recent developments, *Arch. Comput. Methods Eng.* 17 (1) (2010) 25–76.
- [16] V. Leble, G. Barakos, Demonstration of a coupled floating offshore wind turbine analysis with high-fidelity methods, *J. Fluid Struct.* 62 (2016) 272–293.
- [17] B. Ren, M. He, Y. Li, P. Dong, Application of smoothed particle hydrodynamics for modeling the wave-moored floating breakwater interaction, *Appl. Ocean Res.* 67 (2017) 277–290.
- [18] Z. Tan, P.N. Sun, H.G. Lyu, SPH Simulation and Experimental Validation of the Dynamic Response of Moored Floating Bodies under Extreme Wave Conditions, 14th International Conference on Hydrodynamics, Wuxi, China, 2022.
- [19] Z. Liu, Y. Wang, Numerical studies of submerged moored box-type floating breakwaters with different shapes of cross-sections using SPH, *Coast. Eng.* 158 (2020), 103687.
- [20] Z. Liu, Y. Wang, Numerical investigations and optimizations of typical submerged box-type floating breakwaters using SPH, *Ocean Eng.* 209 (2020).
- [21] J. Cui, X. Chen, P. Sun, Numerical investigation on the hydrodynamic performance of a new designed breakwater using smoothed particle hydrodynamic method, *Eng. Anal. Bound. Elem.* 130 (2021) 379–403.
- [22] W.J. Guo, J.B. Zou, M. He, H.F. Mao, Y. Liu, Comparison of hydrodynamic performance of floating breakwaters with taut, slack, and hybrid mooring systems: an SPH-based preliminary investigation, *Ocean Eng.* 258 (2022).
- [23] Z. Wei, B.L. Edge, R.A. Dalrymple, A. Herault, Modeling of wave energy converters by GPU-SPH and Project Chrono, *Ocean Eng.* 183 (2019) 332–349.
- [24] A.J.C. Crespo, C. Altomare, J.M. Domínguez, J. González-Cao, M. Gómez-Gesteira, Towards simulating floating offshore oscillating water column converters with Smoothed Particle Hydrodynamics, *Coast. Eng.* 126 (2017) 11–26.
- [25] H. Wen, B. Ren, X. Yu, An improved SPH model for turbulent hydrodynamics of a 2D oscillating water chamber, *Ocean Eng.* 150 (2018) 152–166.
- [26] P.W. Cleary, M. Rudman, Extreme wave interaction with a floating oil rig: prediction using SPH, *Prog. Comput. Fluid Dynam. Int. J.* 9 (6–7) (2009) 332–344.
- [27] F. Zhang, L. Zhang, Y. Xie, Z. Wang, S. Shang, Smoothed particle hydrodynamics simulation of a mariculture platform under waves, *Water* 13 (20) (2021).
- [28] R.A. Gingold, J.J. Monaghan, Smoothed particle hydrodynamics: theory and application to non-spherical stars, *Mon. Not. Roy. Astron. Soc.* 181 (2) (1977) 375–389.
- [29] L.B. Lucy, A numerical approach to the testing of the fission hypothesis close binary star formation, *Astron. J.* 82 (12) (1977) 1013–1024.
- [30] S.L. Gu, W.G. Zheng, H.T. Wu, C. Chen, S.D. Shao, DualSPHysics simulations of spillway hydraulics: a comparison between single- and two-phase modelling approaches, *J. Hydraul. Res.* (2022).
- [31] A. Zhang, P.N. Sun, F.R. Ming, An SPH modeling of bubble rising and coalescing in three dimensions, *Comput. Methods Appl. Mech. Eng.* 294 (2015) 189–209.
- [32] T. Long, D. Hu, D.T. Wan, C. Zhuang, G. Yang, An arbitrary boundary with ghost particles incorporated in coupled FEM-SPH model for FSI problems, *J. Comput. Phys.* 350 (2017) 166–183.
- [33] A.M. Zhang, P.N. Sun, F.R. Ming, A. Colagrossi, Smoothed particle hydrodynamics and its applications in fluid-structure interactions, *J. Hydraul.* 29 (2) (2017) 187–216.
- [34] F. He, H.S. Zhang, C. Huang, M.B. Liu, Numerical investigation of the solitary wave breaking over a slope by using the finite particle method, *Coast. Eng.* 156 (2020).
- [35] N. Tsuruta, A. Khayyer, H. Gotoh, K. Suzuki, Development of Wavy Interface model for wave generation by the projection-based particle methods, *Coast. Eng.* 165 (2021).
- [36] M. Luo, A. Khayyer, P.Z. Lin, Particle methods in ocean and coastal engineering, *Appl. Ocean Res.* 114 (2021).
- [37] H.J. Wen, B. Ren, P. Dong, G.C. Zhu, Numerical analysis of wave-induced current within the inhomogeneous coral reef using a refined SPH model, *Coast. Eng.* 156 (2020).
- [38] C. Zhang, Y.J. Zhu, Y.C. Yu, D. Wu, M. Rezavand, S.D. Shao, X.Y. Hu, An artificial damping method for total Lagrangian SPH method with application in biomechanics, *Eng. Anal. Bound. Elem.* 143 (2022) 1–13.
- [39] G. Fourtakas, R. Vacondio, J.D. Alonso, B.D. Rogers, Improved Density Diffusion Term for Long Duration Wave Propagation, 2020 SPHERIC Harbin International Workshop, 2020.
- [40] H. Wendland, Piecewise polynomial, positive definite and compactly supported radial functions of minimal degree, *Adv. Comput. Math. (Netherlands)* 4 (4) (1995) 389–396.
- [41] J.J. Monaghan, Smoothed particle hydrodynamics, *Annu. Rev. Astron. Astrophys.* 30 (1) (1992) 543–574.
- [42] J.J. Monaghan, A. Kos, Solitary waves on a Cretan beach, *J. Waterway Port Coastal Ocean Eng.-Asce* 125 (3) (1999) 145–154.
- [43] A. Colagrossi, M. Antuono, D. Le Touze, Theoretical considerations on the free-surface role in the smoothed-particle-hydrodynamics model, *Phys. Rev.* 79 (5) (2009).
- [44] P.W. Randles, L.D. Libersky, Smoothed particle hydrodynamics: some recent improvements and applications, *Comput. Methods Appl. Mech. Eng.* 139 (1–4) (1996) 375–408.
- [45] L.D. Libersky, A.G. Petschek, T.C. Carney, J.R. Hipp, F.A. Allahdadi, High strain Lagrangian hydrodynamics: a three-dimensional SPH code for dynamic material response, *J. Comput. Phys.* 109 (1) (1993) 67–75.
- [46] S. Adami, X.Y. Hu, N.A. Adams, A generalized wall boundary condition for smoothed particle hydrodynamics, *J. Comput. Phys.* 231 (21) (2012) 7057–7075.
- [47] A.J.C. Crespo, M. Gomez-Gesteira, R.A. Dalrymple, Boundary conditions generated by dynamic particles in SPH methods, *Cmc-Computers Materials & Continua* 5 (3) (2007) 173–184.
- [48] B. Bouscasse, A. Colagrossi, S. Marrone, M. Antuono, Nonlinear water wave interaction with floating bodies in SPH, *J. Fluid Struct.* 42 (2013) 112–129.
- [49] P.N. Sun, F.R. Ming, A. Zhang, Numerical simulation of interactions between free surface and rigid body using a robust SPH method, *Ocean Eng.* 98 (2015) 32–49.
- [50] M. Mabsout, M.I. Herreros, Runge-Kutta vs Taylor-SPH: two time integration schemes for SPH with application to Soil Dynamics, *Appl. Math. Model.* 37 (5) (2013) 3541–3563.
- [51] J.M. Domínguez, A.J.C. Crespo, M. Gomez-Gesteira, J.C. Marongiu, Neighbour lists in smoothed particle hydrodynamics, *Int. J. Numer. Methods Fluid.* 67 (12) (2011) 2026–2042.
- [52] A.J.C. Crespo, J.M. Domínguez, B.D. Rogers, M. Gomez-Gesteira, S. Longshaw, R. Canelas, R. Vacondio, A. Barreiro, O. García-Feal, DualSPHysics: open-source parallel CFD solver based on smoothed particle hydrodynamics (SPH), *Comput. Phys. Commun.* 187 (2015) 204–216.
- [53] J.M. Domínguez, A.J.C. Crespo, D. Valdez-Balderas, B.D. Rogers, M. Gomez-Gesteira, New multi-GPU implementation for smoothed particle hydrodynamics on heterogeneous clusters, *Comput. Phys. Commun.* 184 (8) (2013) 1848–1860.
- [54] J.M. Domínguez, A.J.C. Crespo, M. Hall, C. Altomare, M. Wu, V. Stratigaki, P. Troch, L. Cappietti, M. Gómez-Gesteira, SPH simulation of floating structures with moorings, *Coast. Eng.* 153 (2019).
- [55] M. Hall, A. Goupee, Validation of a lumped-mass mooring line model with DeepCwind semisubmersible model test data, *Ocean Eng.* 104 (2015) 590–603.
- [56] J.M. Domínguez, G. Fourtakas, C. Altomare, R.B. Canelas, A. Tafuni, O. García-Feal, I. Martínez-Estévez, A. Mokos, R. Vacondio, A.J.C. Crespo, B.D. Rogers, P. K. Stansby, M. Gomez-Gesteira, DualSPHysics: from Fluid Dynamics to Multiphysics Problems, Computational Particle Mechanics, 2021.
- [57] A. Robertson, J. Jonkman, M. Masciola, H. Song, A. Goupee, A. Coulling, C. Luan, Definition of the Semisubmersible Floating System for Phase II of OC4, Scitech Connect Definition of the Floating System for Phase IV of Oc3, 2014.